

Conditional Capacity and Transmit Signal Design for SWIPT Systems with Multiple Nonlinear Energy Harvesting Receivers

Rania Morsi, Vahid Jamali, Amelie Hagelauer, Derrick Wing Kwan Ng,
and Robert Schober

Abstract—In this paper, we study information-theoretic limits for simultaneous wireless information and power transfer (SWIPT) systems employing practical nonlinear radio frequency (RF) energy harvesting (EH) receivers (Rxs). In particular, we consider a SWIPT system with one transmitter that broadcasts a common signal to an information decoding (ID) Rx and multiple EH Rxs. Owing to the nonlinearity of the EH Rxs' circuitry, the efficiency of wireless power transfer depends on the waveform of the transmitted signal. We aim to answer the following fundamental question: *What is the optimal input distribution of the transmit signal waveform that maximizes the information transfer rate at the ID Rx conditioned on individual minimum required direct-current (DC) powers to be harvested at the EH Rxs?* Specifically, we study the conditional capacity problem of a SWIPT system impaired by additive white Gaussian noise subject to average-power (AP) and peak-power (PP) constraints at the transmitter and nonlinear EH constraints at the EH Rxs. To this end, we develop a novel nonlinear EH model that captures the saturation of the harvested DC power by taking into account not only the forward current of the rectifying diode but also the reverse breakdown current. Then, we derive a novel semi-closed-form expression for the harvested DC power, which simplifies to closed form for low input RF powers. The derived analytical expressions are shown to closely match circuit simulation results. We solve the conditional capacity problem for real- and complex-valued signalling and prove that the optimal input distribution that maximizes the rate-energy (R-E) region is unique and discrete with a finite number of mass points. Furthermore, we show that, for the considered nonlinear EH model and a given AP constraint, the boundary of the R-E region saturates for high PP constraints due to the saturation of the harvested DC power for high input RF powers. In addition, we devise a suboptimal input distribution whose R-E tradeoff performance is close to optimal. All theoretical findings are verified by numerical evaluations.

I. INTRODUCTION

In addition to their capability to convey information, radio frequency (RF) signals can transfer energy for wirelessly charging low-power devices. This property of RF signals has attracted significant attention to the study of simultaneous wireless information and power transfer (SWIPT) systems [2]–[10]. In [2], the author defined a rate-energy (R-E) function that characterizes the tradeoff between wireless information transfer (WIT) and wireless power transfer (WPT). Such a tradeoff exists as long as the optimal transmit waveform that maximizes the rate of information transfer is different from the one that maximizes the amount of harvested energy. For example, in [3], the R-E tradeoff for frequency selective channels with additive white Gaussian noise (AWGN) is characterized, where water-filling power allocation is shown to be optimal for WIT, but allocating all the power to a single sinusoid is optimal for WPT. In [4], it is shown that for a multi-antenna broadcast channel, spatial multiplexing is optimal for WIT, whereas energy beamforming is optimal for WPT. The aforementioned works lay the foundation for SWIPT research, but they are based on an overly simplistic linear energy harvesting (EH) model for WPT. This model assumes that the harvested direct-current (DC) power depends only on the *average* power of the input RF signal and that this dependence is *linear* for all possible input RF powers.

In practice, however, the RF EH circuits of WPT systems have a nonlinear input-output characteristic [11]–[19]. In particular, EH circuits include a rectenna, i.e., an antenna followed by a rectifier. The rectifier typically contains diodes followed by a capacitor-based low-pass filter (LPF) to convert the received RF signal into a DC signal. For high incident RF powers, rectifying diodes exhibit the reverse breakdown phenomenon, where a significant amount of reverse current flows through the diode causing the output DC power to saturate and leading to a reduced RF-to-DC conversion efficiency [14], [15]. In [13], the nonlinear RF-to-DC input-output characteristic of a rectenna is modelled by a three-parameter sigmoidal function, where curve fitting is performed to determine the parameters for a given rectenna circuit and a given excitation signal.

In this paper, we adopt the same rectifier circuit as was considered in [17]–[19], namely a series single-diode rectifier. In [17], a monotonically increasing function of the

R. Morsi, V. Jamali, and R. Schober are with the Institute for Digital Communications, and A. Hagelauer is with the Institute for Electronics Engineering in Friedrich-Alexander University (FAU), Erlangen, Germany. D. W. K. Ng is with the University of New South Wales, Australia. (E-mails: rania.morsi@fau.de; vahid.jamali@fau.de; amelie.hagelauer@fau.de; w.k.ng@unsw.edu.au; robert.schober@fau.de)

This paper was presented in part in [1] at the IEEE International Conference on Communications (ICC), Kansas City, USA, 2018.

D. W. K. Ng is supported by funding from the UNSW Digital Grid Futures Institute, UNSW, Sydney, under a cross-disciplinary fund scheme and by the Australian Research Council's Discovery Early Career Researcher Award (DE170100137). Robert Schober's work is supported by DFG project SCHO 831/12-1.

output DC power is derived in terms of an integral function of the input RF signal. In [18], a fourth-order Taylor series approximation of the expression in [17] is analyzed for a multisine excitation signal. Furthermore, the authors of [19] obtained a semi-closed-form expression for the output DC voltage assuming a sinusoidal input RF signal. However, the analysis in the aforementioned works [17]–[19] took into account only the forward-bias current-voltage (I-V) characteristic of the rectifying diode, as described by Shockley’s diode equation [20]. This model ignores the reverse-breakdown behaviour of the diode and therefore does not capture the saturation of the output DC power for high input RF powers. In contrast, in this paper, we take into account both the forward and the reverse breakdown I-V characteristic of the rectifying diode and obtain a novel semi-closed-form expression for the output DC power assuming a sinusoidal input excitation signal. Moreover, in the low-input power regime, we obtain the output DC power in closed form. A comparison with circuit simulations confirms the accuracy of the derived analytical expressions.

Owing to the rectifier’s nonlinearity, the RF-to-DC conversion efficiency depends not only on the strength of the input RF signal, but also on its waveform [15]–[18]. For example, experiments have shown that signals with high peak-to-average power ratio (PAPR), such as multisine signals, yield higher harvested DC powers for a given average incident RF power compared to constant-envelope signals [16]. This is because, for low average power levels, high PAPR signals are more likely to exceed the turn-on voltage of the diode [15]. Moreover, the peaks of a high PAPR signal can charge the capacitor to a high voltage level, and if the output LPF has a large time constant, the capacitor can maintain the charged voltage until the next signal peak, see e.g. [16, Figure 9]. Thus, the nonlinearity of EH circuits motivates the optimization of the transmit signal for maximization of the amount of harvested energy.

While the goal of waveform design for a pure WPT system is to maximize the harvested energy only, for a SWIPT system, the waveform design goal is to maximize both the information transfer rate and the harvested energy, i.e., to optimize the R-E tradeoff. In [8], the R-E tradeoff of different receiver (Rx) architectures is studied for SWIPT systems with a nonlinear EH model. In [9], the authors consider the superposition of deterministic and modulated multisine waveforms and optimize the amplitudes and phases of all frequency tones to maximize the R-E region, i.e., the region of all achievable R-E pairs. As an alternative to using multisine signals, the desired high PAPR characteristic of WPT signals can also be achieved by modulating the amplitude of a single-sine signal. Thereby, the amplitude modulation can be simultaneously used to transmit information. From the WPT perspective, the optimal distribution of the transmit amplitude is expected to have a high PAPR. On the other hand, from a WIT perspective, the optimal distribution of the transmit amplitude is known to be Gaussian for an average power limited AWGN channel [21]. Hence, the

aim of this paper is to answer the following fundamental question. “*For a single-carrier SWIPT system with a nonlinear EH circuit, what is the optimal input distribution of the transmit waveform that maximizes the R-E region?*”

First steps towards answering this question are made in [10], where input distributions that are fully characterized by their first- and second-order statistics are considered. It is shown that, in this case, the optimal input distribution is the zero-mean complex Gaussian distribution with asymmetric power allocation to the real and imaginary parts. However, in general, higher-order statistics may be required to characterize the optimal input distribution that maximizes the R-E region, in which case the waveforms reported in [10] are no longer optimal.

In this paper, we aim to answer the question above without limiting ourselves to input distributions that are fully characterized by their first- and second-order statistics. In particular, we consider a SWIPT system, where a single-carrier signal is transmitted over AWGN channels to an information decoding (ID) Rx and simultaneously to multiple EH Rxs. Our objective is to find the optimal distribution of the transmit signal that maximizes the information rate at the ID Rx under individual minimum harvested power constraints at the nonlinear EH Rxs. To specify the EH constraints, we employ the harvested DC power function derived for our newly developed nonlinear EH saturation model. In addition, we impose average-power (AP) and peak-power (PP) constraints at the power transmitter¹. We note that, for a linear EH model, the considered problem is trivial since, in this case, the harvested DC power depends only on the average input RF power, which renders the input distribution of the transmit symbols irrelevant for WPT. In particular, in addition to the commonly adopted maximum AP constraint, the linear EH constraint imposes a minimum AP constraint, for which the problem is either infeasible or the EH constraint is inactive. In the latter case, the solutions for maximum WIT in [21]–[23] are optimal. On the other hand, with a nonlinear EH model, this problem is non-trivial and has been first studied in our preliminary work in [1], for one EH Rx². Subsequently, a similar problem has been independently studied in [24] using the nonlinear EH model from [18], which does not model the saturation of the output DC power but adopts a 4th-order truncated Taylor series approximation of the diode’s forward current equation.

The main contributions of this paper can be summarized as follows:

- We study the conditional capacity of a SWIPT system with one ID Rx and multiple nonlinear EH Rxs. In particular, we maximize the information rate at the ID Rx under AP and PP constraints at the transmitter and nonlinear EH constraints at the EH Rxs. Accordingly, we obtain the R-E region, which

¹This problem is of practical interest in e.g. sensor networks where one sensor needs to update its software at the highest possible rate while the other sensors in its vicinity want to wirelessly charge their batteries.

²The work in [1] was first published in Nov. 2017, see <https://arxiv.org/abs/1711.01082>.

specifies all combinations of achievable rates at the ID Rx and jointly feasible harvested powers at the EH Rxs. The boundary of this R-E region is referred to as the R-E tradeoff curve.

- We obtain necessary and sufficient conditions for the optimal input distribution and prove that it is unique and discrete with a finite number of mass points. The discreteness and finiteness of optimal input distributions for other channels have been reported in [22], [23], [25]–[27].
- Different from our preliminary work in [1], in this paper, we additionally consider the following:
 - In order to accurately model the harvested DC power, we take into account not only the forward but also the reverse breakdown I-V characteristic of the rectifying diode. Consequently, the proposed nonlinear EH model captures the saturation behaviour of the output DC power at high input RF powers. Moreover, our model includes the voltage multiplication effect of the matching network that maximizes the power transfer from the antenna to the rectifier. Accordingly, we obtain a semi-closed-form expression of the output DC power. In addition, in the low input RF power regime, the forward I-V characteristic of the diode is dominant and the harvested DC power is obtained in closed form. The derived analytical expressions are verified with circuit simulations and exploited to formulate the EH constraints for the R-E region maximization problem.
 - We consider multiple EH Rxs with individual minimum EH constraints and prove that, if none of the EH Rxs operates in saturation, at most one of these EH constraints is active. In particular, the active EH constraint is the one which, when all other EH constraints are removed, results in the smallest achievable rate at the ID Rx. Hence, the R-E tradeoff curve for this problem is completely characterized by the individual R-E curves obtained for each individual EH Rx separately.
 - We extend the problem to complex-valued transmission and show that the optimal input distribution is characterized by a discrete and finite amplitude set with an independent uniformly distributed phase. This result is in line with the results for the same problem without EH constraints in [23].
 - We solve the problem of maximum WPT for one EH Rx under AP and PP constraints. We obtain the optimal input distribution and the maximum harvested DC power at the EH Rx in closed form. We show that on-off transmission is optimal for maximum WPT. Based on this insight, for the SWIPT system, we propose a suboptimal distribution which superimposes the optimal distributions for maximum WPT and maximum WIT. We show that the R-E tradeoff obtained with the suboptimal distribution closely approaches that of the optimal one.
 - We show that, owing to the saturation behaviour

of the harvested DC power, the optimal solution for maximum WPT and the boundary of the R-E region saturate for high PP constraints.

The remainder of the paper is organized as follows. In Section II, we present the system model and the nonlinear EH circuit model. In Section III, we formulate the R-E problem and reveal several properties of the optimal input distribution. In Section IV, we study the extreme problems of maximum WIT and maximum WPT and propose a suboptimal input distribution for the SWIPT problem. In Section V, we provide numerical results for the considered problems. Finally, Section VI concludes the paper.

Notations: We use boldface letters to denote random variables and the corresponding lightface letters to denote their realizations. j is the imaginary unit and $\Re\{\cdot\}$ denotes the real part of a complex number. $\mathbb{E}_F[V(\mathbf{x})] = \int V(\mathbf{x})dF(\mathbf{x})$ is the statistical average of $V(\mathbf{x})$ given that random variable \mathbf{x} has distribution function $F(\mathbf{x})$. Moreover, \sim stands for “is distributed as” and \triangleq means “is defined as”. $\mathcal{N}(0, \sigma^2)$ and $\mathcal{CN}(0, \sigma^2)$ represent real- and complex-valued Gaussian distributions with zero mean and variance σ^2 .

II. SYSTEM MODEL AND PRELIMINARIES

A. System Model

We consider a single-antenna SWIPT system, where a transmitter broadcasts a common single-carrier signal to an ID Rx and L randomly deployed EH Rxs, as shown in Fig. 1. In particular, we consider a time-slotted system with time slot duration³ T . The transmitter emits a real-valued⁴ baseband information-bearing pulse-amplitude modulated signal $x(t) = \sum_{k=-\infty}^{\infty} x[k]g(t-kT)$, where $g(t)$ is the transmit pulse waveform and $x[k]$ is the information-bearing symbol in time slot k , which is a realization of an independent and identically distributed (i.i.d.) real-valued random variable $\mathbf{x} \in \mathbb{R}$ having cumulative distribution function F . The channel gains for the ID and EH Rxs are denoted by $h_I \in \mathbb{R}$ and $h_{E_l} \in \mathbb{R}$, respectively, and are assumed to be fixed over all time slots, where $l \in \mathcal{L} \triangleq \{1, \dots, L\}$. To obtain an upper bound on the performance of the SWIPT system, all channel gains are assumed to be perfectly known at the transmitter⁵ and the information channel gain is known at the ID Rx. The baseband model of the received signal at the ID Rx is given by $y_I(t) = x(t)h_I + n(t)$, where $n(t)$ is real-valued AWGN with average power σ_n^2 . At the EH Rxs, the additive noise is ignored since its contribution to the harvested power is negligible.

³In this paper, we assume a unit-length time slot, i.e., $T = 1$. Hence, we use the terms power and energy interchangeably.

⁴As is customary for capacity analysis, see e.g. [22], [26], [27], as a first step, we assume real-valued channel inputs and outputs. The generalization to a complex-valued signal model is provided in Section IV-D.

⁵In practice, assuming a time-division duplex (TDD) system, for channel acquisition, the ID and EH nodes may transmit pilot signals to the transmitting node, which then estimates the uplink channel gains and exploits the uplink-downlink channel reciprocity to obtain estimates for the downlink channel gains.

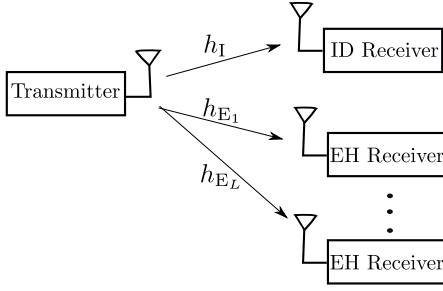


Fig. 1: SWIPT system with one ID Rx and L separate EH Rxs.

Hence, at the l^{th} EH Rx, the received signals in the baseband and the RF domains are $y_{E_l}(t) = x(t)h_{E_l}$ and $y_{E_l}^{\text{RF}}(t) = \sqrt{2}\Re\{y_{E_l}(t)e^{j2\pi f_c t}\}$, respectively, where f_c is the carrier frequency and $w_c \triangleq 2\pi f_c$ is the corresponding angular frequency. Assuming a rectangular pulse $g(t)$ with unit amplitude and duration T , in time slot k , i.e., $kT - T/2 < t \leq kT + T/2$, the baseband transmit signal is constant and given by $x(t) = \sum_{k=-\infty}^{\infty} x[k]g(t - kT) = x[k]$. Assuming all EH Rxs employ identical EH circuits, we focus on modelling one EH Rx and drop index l , for convenience. Thus, the received RF signal at the EH Rx is

$$y_E^{\text{RF}}(t) = \sqrt{2}x[k]h_E \cos(2\pi f_c t), \quad kT - T/2 < t \leq kT + T/2. \quad (1)$$

B. Rectenna Nonlinear Circuit Model

In this section, we derive a novel expression for the harvested DC power at the EH Rx averaged over the symbol duration T in which symbol x is transmitted. As shown in Fig. 2, the EH Rx includes a rectenna, which consists of an antenna and a rectifier. The antenna is commonly modelled by a Thevenin equivalent voltage source $v_s(t)$ in series with an impedance R_{ant} [15], [17]–[19]. The rectifier converts the received RF signal to a DC signal across a load resistance R_L . In order to ensure maximum power transfer, a matching network is needed to match the rectifier's input impedance Z_a to the antenna impedance R_{ant} , cf. Fig. 2. Since the received RF signal $y_E^{\text{RF}}(t)$ given in (1) is sinusoidal, it follows that signals $v_s(t)$, $v_b(t)$, and $v_a(t)$ in Fig. 2 are also sinusoidal. In the following, we use the notation \hat{v} to denote the peak amplitude of sinusoidal signal $v(t)$, i.e., $v(t) = \hat{v} \cos(2\pi f_c t + \phi_v)$, where $v \in \{y_E^{\text{RF}}, v_s, v_b, v_a\}$ and $\phi_v \in [-\pi, \pi]$. We adopt the rectifier circuit used in [17]–[19], which consists of a single series diode followed by a capacitor-based LPF with capacitance C_L . Unlike in [17] and [18], our model includes the diode's series resistance R_s and junction capacitance C_j , see Fig. 2, [19, Fig. 1], [15, Fig. 5.2]. The main differences between the rectifier model developed in this paper and the models in [17]–[19] are:

1) *Saturation Circuit Model*: First, we derive the harvested DC power at the rectifier's output in terms of the peak voltage \hat{v}_a at the rectifier's input. To this end, we consider not only the forward-bias mode of the rectifying diode but also the reverse-bias breakdown mode. A typical I-V characteristic of a rectifying diode is

shown in [15, Fig. 6.5]. In particular, when the amplitude of the voltage signal across the diode junction $v_{d_j}(t)$ reaches the diode breakdown voltage B_v , a significant amount of reverse current will pass through the diode for negative values of the input signal. This leads to a reduction of the average current in the diode, the saturation of the output DC power, and a degradation of the RF-to-DC power conversion efficiency as the input signal power increases [15]. In order to account for this nonlinear behaviour of the diode current, the total current in the diode junction $i_{d_j}(t)$ is modelled as the sum of the diode forward current $i_F(t)$ and the reverse current $i_R(t)$, i.e., [15, Eqs. (6.1)–(6.3)]⁶

$$\begin{aligned} i_{d_j}(t) &= i_F(t) + i_R(t) \\ &= I_s \left(e^{\frac{v_{d_j}(t)}{\eta V_T}} - 1 \right) - I_{B_v} e^{-\frac{B_v}{\eta V_T}} \left(e^{-\frac{v_{d_j}(t)}{\eta V_T}} - 1 \right), \end{aligned} \quad (2)$$

where I_s is the diode's reverse bias saturation current, η is the diode ideality factor, which typically lies between 1 and 2, $V_T = KT_K/q$ is the thermal voltage, where K is Boltzmann's constant, q is the electron charge, and T_K is the junction temperature in Kelvin. The reverse breakdown current is characterized by I_{B_v} and B_v , which represent the breakdown saturation current and the reverse breakdown voltage, respectively [15]. Applying Kirchhoff's current law to the rectifier in Fig. 2, we obtain

$$\begin{aligned} i_d(t) &= i_{d_j}(t) + i_{C_j}(t) = i_{C_L}(t) + i_{\text{out}}(t) \\ &= I_s \left(e^{\frac{v_{d_j}(t)}{\eta V_T}} - 1 \right) - I_{B_v} e^{-\frac{B_v}{\eta V_T}} \left(e^{-\frac{v_{d_j}(t)}{\eta V_T}} - 1 \right) + C_j \frac{dv_{d_j}(t)}{dt} \\ &= C_L \frac{dv_{\text{out}}(t)}{dt} + \frac{v_{\text{out}}(t)}{R_L}. \end{aligned} \quad (3)$$

Due to the nonlinearity of the diode detector circuit, the voltage signals $v_{\text{out}}(t)$ and $v_{d_j}(t)$ in (3) contain in general DC and harmonic components [15], [28]. Hence, in the most general sense, we can write $v_z(t) = \sum_{n=0}^{\infty} \hat{v}_z^{(n)} \cos(2\pi n f_c t + \phi_z^{(n)})$, where $z \in \{d_j, \text{out}\}$ and the superscript (n) denotes the n^{th} harmonic component. Thus, $\frac{1}{T} \int_T v_z(t) dt = \hat{v}_z^{(0)}$ and $\frac{1}{T} \int_T \frac{dv_z(t)}{dt} dt = 0$. Therefore, integrating both sides of (3) over one symbol duration T results in

$$\frac{1}{T} \int_T \left[I_s \left(e^{\frac{v_{d_j}(t)}{\eta V_T}} - 1 \right) - I_{B_v} e^{-\frac{B_v}{\eta V_T}} \left(e^{-\frac{v_{d_j}(t)}{\eta V_T}} - 1 \right) \right] dt = \frac{V_{\text{out}}}{R_L}, \quad (4)$$

where we define $V_{\text{out}} \triangleq \hat{v}_{\text{out}}^{(0)}$. Assuming the rectifier's time constant $R_L C_L$ is much larger than the period $1/f_c$ of the sinusoidal RF signal, the ripples in the output voltage will be negligible [15]. In this case, at steady state, the output voltage can be assumed constant (DC), i.e., $v_{\text{out}}(t) = V_{\text{out}}$ and $i_d(t) = C_L \frac{dv_{\text{out}}(t)}{dt} + \frac{v_{\text{out}}(t)}{R_L} = \frac{V_{\text{out}}}{R_L}$. Hence, the junction voltage in (4) can be written as $v_{d_j}(t) = v_a(t) - i_d(t)R_s - v_{\text{out}}(t) = v_a(t) - V_{\text{out}} \left(1 + \frac{R_s}{R_L} \right)$

⁶In [15, Eq. (6.2)], the last term $I_{B_v} e^{-\frac{B_v}{\eta V_T}}$ in (2) is set to zero, which is valid for typical rectifying diodes, see e.g. [15, Table 5.4].

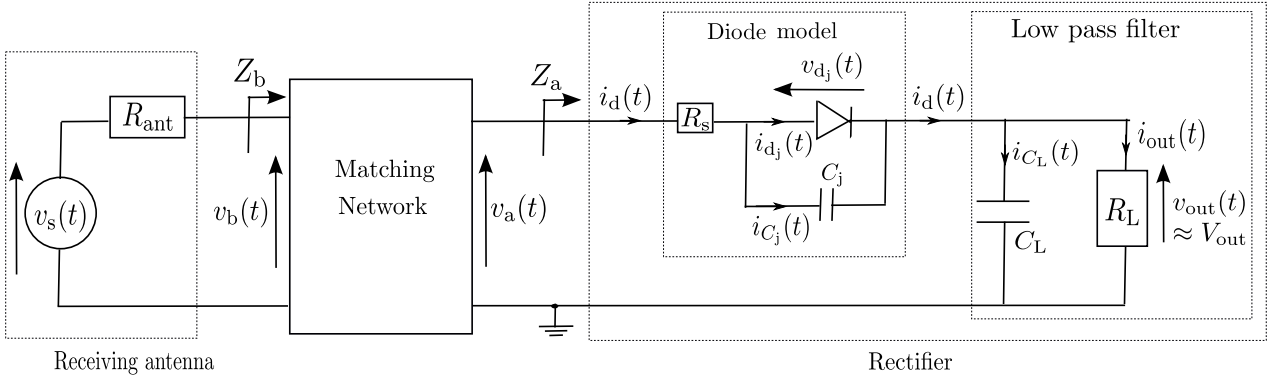


Fig. 2: Nonlinear rectenna circuit model.

and (4) reduces to

$$I_s \left[e^{\frac{-V_{out}(\beta)}{\eta V_T} \left(1 + \frac{R_s}{R_L}\right)} I_0(\beta) - 1 \right] - I_{B_v} e^{-\frac{B_v}{\eta V_T}} \left[e^{\frac{V_{out}(\beta)}{\eta V_T} \left(1 + \frac{R_s}{R_L}\right)} I_0(\beta) - 1 \right] = \frac{V_{out}(\beta)}{R_L}, \quad (5)$$

where $\beta \triangleq \frac{\hat{v}_a}{\eta V_T}$ and the notation $V_{out}(\beta)$ is used to explicitly indicate the dependence of V_{out} on β . To arrive at (5), we assumed $f_c = m/T$, with integer m , in order to use $I_0(\beta) = \frac{1}{T} \int_T e^{\beta \cos(2\pi \frac{m}{T} t + \phi_{v_a})} dt$, where $I_0(\cdot)$ is the modified Bessel function of the first kind and order zero. Given the amplitude of the voltage signal at the rectifier's input, \hat{v}_a , and therefore β , (5) is a semi-closed-form expression for the DC voltage $V_{out}(\beta)$, which can be solved using e.g. Newton's method. Then, the harvested DC power is

$$P_{out}(\beta) \Big|_{\text{exact}} = \frac{V_{out}^2(\beta)}{R_L}, \quad V_{out}(\beta) \text{ is the solution of (5).} \quad (6)$$

Remark 1. We note that, for low input RF powers, the amplitude of the diode junction voltage $v_{dj}(t)$ is small and does not reach the breakdown voltage of the diode. Hence, the reverse current in (2) becomes negligible, i.e., $i_R(t) \approx 0$. In this case, the diode current in (2) reduces to the well-known Shockley diode equation given by $i_{dj}(t) = i_F(t) = I_s (e^{\frac{v_{dj}(t)}{\eta V_T}} - 1)$ [20]. Consequently, the second bracketed term on the left hand side (LHS) of (5) tends to zero. Thus, in the low input power regime, (5) reduces to

$$I_0(\beta) = \left(1 + \frac{V_{out}}{I_s R_L}\right) e^{\frac{V_{out}}{\eta V_T} \left(1 + \frac{R_s}{R_L}\right)}, \quad (7)$$

which was given in [19, Eq. (15)]. Multiplying both sides of (7) by $\frac{I_s(R_L + R_s)}{\eta V_T} e^{\frac{I_s(R_L + R_s)}{\eta V_T}}$, we get

$$\frac{I_s(R_L + R_s)}{\eta V_T} e^{\frac{I_s(R_L + R_s)}{\eta V_T}} I_0(\beta) = \frac{I_s(R_L + R_s)}{\eta V_T} \left(1 + \frac{V_{out}}{I_s R_L}\right) e^{\frac{I_s(R_L + R_s)}{\eta V_T} \left(1 + \frac{V_{out}}{I_s R_L}\right)}. \quad (8)$$

The right hand side (RHS) of (8) has the form $w e^w$, where $w = \frac{I_s(R_L + R_s)}{\eta V_T} \left(1 + \frac{V_{out}}{I_s R_L}\right)$. Since function $w e^w$ is invertible for $w e^w \in [0, \infty)$ and the LHS of (8) is $\in [0, \infty)$, the unknown w has a unique solution given

by $w = W_0(a e^a I_0(\beta))$, where $a = \frac{I_s(R_L + R_s)}{\eta V_T}$ and $W_0(\cdot)$ is the principal branch of the LambertW function [29]. Hence, for low input RF powers, V_{out} can be obtained in closed form as $V_{out}(\beta) = \left[\frac{1}{a} W_0(a e^a I_0(\beta)) - 1\right] I_s R_L$ and the harvested DC power $P_{out}(\beta) = V_{out}^2(\beta)/R_L$ reduces to⁷

$$P_{out}(\beta) \Big|_{\text{low power}} = \left[\frac{1}{a} W_0(a e^a I_0(\beta)) - 1\right]^2 I_s^2 R_L. \quad (9)$$

2) Matching Network Model: In Section II-B1, we obtained the output DC power in terms of the amplitude of the signal at the rectifier's input. In this section, we obtain the output DC power in terms of the power of the RF input signal received by the antenna. To this end, it is essential to model the power transfer from the antenna to the rectifier. This power transfer is maximized by a complex-conjugate matching network that matches the rectifier input impedance⁸ Z_a to the antenna impedance R_{ant} [15, Section 5.3.3]⁹. In particular, let $\{Z_b, v_b(t)\}$ and $\{Z_a, v_a(t)\}$ be the input impedance and the voltage signal *before* and *after* the matching network, respectively, cf. Fig. 2. Then, average power conservation during one symbol duration assuming a lossless matching network implies

$$\Re \left\{ \frac{1}{T} \int_T \frac{|v_a(t)|^2}{Z_a^*} dt \right\} = \Re \left\{ \frac{1}{T} \int_T \frac{|v_b(t)|^2}{Z_b^*} dt \right\} \quad (10)$$

$$\Rightarrow \frac{1}{2} \hat{v}_a^2 \Re \left\{ \frac{1}{Z_a^*} \right\} = \frac{1}{2} \hat{v}_b^2 \Re \left\{ \frac{1}{Z_b^*} \right\}.$$

For perfect matching, $Z_b = R_{ant}$ and $\hat{v}_a = \hat{v}_b / \sqrt{\Re\{R_{ant}/Z_a^*\}}$. Since Z_a is typically larger than R_{ant} , it follows that the amplitude of the voltage signal at

⁷In [30, Eq. (22)], the output DC power is expressed in terms of the LambertW function of an integral involving the received signal. Unlike the analysis in this paper, [30, Eq. (22)] considers only the diode's forward current, uses an approximation of Shockley's diode equation, assumes perfect matching between the antenna and the rectifier, and assumes a zero diode series resistance, i.e., $R_s = 0$.

⁸Note that the rectifier's input impedance Z_a is not only frequency dependent but also input power dependent. Hence, in general, the matching network should be tuned to the RF input power.

⁹As seen from the antenna side, the matching network typically includes a series capacitor that acts as a DC block followed by a shunt inductor that acts as a DC feed providing a DC return path for the rectified current [16, Fig. 2]. Otherwise, the rectified current would pass through the RF signal generator (the antenna) and a part of the rectified power would be consequently lost in the antenna [15], [19], [28].

the output of the matching network is higher than that at its input, i.e., $\hat{v}_a > \hat{v}_b$ [31]. Hence, the matching network effectively acts as a voltage multiplier.

Next, we obtain relationships between the input RF power and the signal peak amplitudes \hat{y}_E^{RF} , \hat{v}_s , \hat{v}_b , and \hat{v}_a . In particular, for perfect matching, the average received RF power captured by the antenna during one time slot, denoted by P_{in} , is completely transferred to the rectifier, i.e., $P_{\text{in}} = \frac{1}{T} \int_T |y_E^{\text{RF}}(t)|^2 dt = \frac{1}{T} \int_T |v_b(t)|^2 / R_{\text{ant}} dt$, or equivalently $\hat{v}_b = \hat{y}_E^{\text{RF}} \sqrt{R_{\text{ant}}}$. Hence, $\hat{v}_a = \hat{y}_E^{\text{RF}} / \sqrt{\Re\{1/Z_a^*\}}$. Assuming symbol x is transmitted in the time slot under consideration, then from (1), $\hat{y}_E^{\text{RF}} = \sqrt{2}xh_E$ and the average input power of the received RF signal, P_{in} , can be written as

$$P_{\text{in}} = \frac{1}{2} (\hat{y}_E^{\text{RF}})^2 = (xh_E)^2 = \frac{1}{2} \frac{\hat{v}_b^2}{R_{\text{ant}}} = \frac{1}{2} \hat{v}_a^2 \Re\left\{\frac{1}{Z_a^*}\right\} = \frac{\hat{v}_s^2}{8R_{\text{ant}}}, \quad (11)$$

where we used $\hat{v}_b = \hat{v}_s/2$ for perfect matching. Using (11) and defining $B \triangleq 1/(\eta V_T \sqrt{\Re\{1/Z_a^*\}})$, then the argument of the modified Bessel function, $\beta = \frac{\hat{v}_a}{\eta V_T}$, defined in (5) can be written as

$$\beta = \frac{\hat{v}_a}{\eta V_T} = B \hat{y}_E^{\text{RF}} = B \frac{\hat{v}_b}{\sqrt{R_{\text{ant}}}} = B \sqrt{2P_{\text{in}}} = \sqrt{2} B h_E x. \quad (12)$$

Using (12), the harvested DC power in (6) and (9) can be expressed in terms of the input power P_{in} , the transmit symbol x , and the peak amplitudes \hat{v}_a , \hat{y}_E^{RF} , \hat{v}_b . However, from (12), this requires the knowledge of $B = 1/(\eta V_T \sqrt{\Re\{1/Z_a^*\}})$ and therefore the input impedance of the rectifier Z_a . According to the diode model in [28, Fig. 12], the diode junction can be modelled as a variable resistor R_d whose value depends on the input RF power. Hence, the rectifier input impedance Z_a in Fig. 2 can be written as

$$Z_a(R_d) = R_s + [1/R_d + j\omega_c C_j]^{-1} + [1/R_L + j\omega_c C_L]^{-1}. \quad (13)$$

It was shown in [28] that for small input RF powers, $R_d \rightarrow R_{j0} \triangleq \eta V_T / I_s$, whereas for high input RF powers, $R_d \rightarrow R_L/2$, see [28, caption of Fig. 12, Eq. (49), and Fig. 10(a)]. Note that, C_j depends on the output DC voltage [28, Eq. (2)]. However, we use the approximation $C_j \approx C_{j0}$, where C_{j0} is the diode's junction capacitance at zero output DC voltage provided in the diode's datasheet [28]. As will be shown in Section V, these approximations provide DC powers close to those obtained by circuit simulations.

Remark 2. Note that if perfect matching between the antenna and the rectifier is assumed without including a matching network, as was done in [17] and [18], the voltage multiplication in (10) is not included in the model, i.e., $\hat{v}_a = \hat{v}_b$ is assumed, which leads to an underestimation of the actual harvested DC power.

3) *Approximate Saturation Model:* In [15, Section 6.5.1], it is shown that for very high input RF powers, the DC output voltage of the diode detector in Fig. 2 saturates at $V_{\text{out}}|_{\text{max}} = B_v/2$. Hence, the saturated harvested DC power is given by $P_{\text{out}}|_{\text{max}} = B_v^2/(4R_L)$ [15, Eq. (6.5)].

Since the solution of the saturation model in (5) cannot be obtained in closed form, we combine the low-power approximate solution in (9) with $P_{\text{out}}|_{\text{max}}$ to obtain an approximate solution for the saturation model, namely

$$P_{\text{out}}(\beta)|_{\text{approx.}} = \min\left(\left[\frac{1}{a} W_0(ae^a I_0(\beta)) - 1\right]^2 I_s^2 R_L, \frac{B_v^2}{4R_L}\right). \quad (14)$$

Using (12), we write the harvested DC power in terms of transmit symbol x for the l^{th} EH Rx as

$$P_l(x) \triangleq P_{\text{out}}(\sqrt{2} B h_{E_l} x)|_{\text{approx.}} = \min\left(\left[\frac{1}{a} W_0(ae^a I_0(\sqrt{2} B h_{E_l} x)) - 1\right]^2 I_s^2 R_L, \frac{B_v^2}{4R_L}\right), \quad (15)$$

where $B = 1/(\eta V_T \sqrt{\Re\{1/Z_a(R_{j0})^*\}})$, i.e., we use the low-power approximation of the rectifier's input impedance¹⁰. Our numerical results in Section V confirm that both the exact and the approximate output DC power functions in (6) and (14), respectively, are in good agreement with circuit simulations, cf. Fig. 4. Hence, both expressions may be used for the EH constraints of the SWIPT problem. For notational simplicity, in the following, we will use (15) for the EH constraints of the conditional capacity SWIPT problem. Next, we derive the input RF power $P_{\text{in,sat}}$ at which the output DC power starts to saturate. From (14), saturation of the output DC power occurs when $[\frac{1}{a} W_0(ae^a I_0(\beta)) - 1]^2 I_s^2 R_L = \frac{B_v^2}{4R_L}$. Using (11), (12), we obtain

$$P_{\text{in,sat}} = \left(\frac{\beta_{\text{sat}}}{\sqrt{2} B}\right)^2 = \frac{1}{2} (\eta V_T \beta_{\text{sat}})^2 \Re\left\{\frac{1}{Z_a^*(R_{j0})}\right\}, \quad (16)$$

where β_{sat} is the solution of $I_0(\beta_{\text{sat}}) = e^{\frac{a B_v}{2 I_s R_L}} (1 + B_v/(2 I_s R_L))$. In Table I, we summarize the main results of the saturation model derived in this section.

C. Amplitude Constraints for the Transmitter and the EH Rxs

At the transmitter, the PP is usually limited to avoid the negative impact of power amplifier nonlinearities, i.e., we set $|x| \leq A_T$. Moreover, it may be desired to limit the peak amplitude of the received RF signal at EH Rx l to some value A_{R_l} , i.e., $\hat{y}_{E_l}^{\text{RF}} = |\sqrt{2} x h_{E_l}| \leq A_{R_l}$. Considering the PP constraints at the transmitter and all L EH Rxs, the effective amplitude (or PP) constraint on the transmit signal reduces to

$$|x| \leq \min\left(A_T, \min_{l \in \mathcal{L}} A_{R_l} / |\sqrt{2} h_{E_l}|\right) \triangleq A. \quad (17)$$

For example, setting the maximum received amplitude to $A_{R_{\text{sat}_l}} \triangleq \sqrt{2 P_{\text{in,sat}}}$, $\forall l \in \mathcal{L}$, ensures that

¹⁰We note that the harvested DC power function in (15) depends on the circuit parameters R_s , C_j , C_L , and R_L since $P_l(x)$ is a function of $B = 1/(\eta V_T \sqrt{\Re\{1/Z_a(R_{j0})^*\}})$ and the rectifier's input impedance $Z_a(R_{j0})$ in (13) is a function of these circuit parameters.

none of the EH Rxs operates in saturation¹¹. In this case, the maximum transmit amplitude A is given by $A_{\text{sat}} \triangleq \min(A_T, \min_{l \in \mathcal{L}} A_{T, \text{sat}_l})$, where $A_{T, \text{sat}_l} \triangleq A_{R, \text{sat}_l} / |\sqrt{2}h_{E_l}| = \sqrt{P_{\text{in}, \text{sat}} / |h_{E_l}|}$.

Using the closed-form expression for the harvested DC power in (15) and the PP constraint in (17), we formulate next the conditional capacity problem of the SWIPT system in Fig. 1.

III. PROBLEM FORMULATION AND SOLUTION

In this section, we study the conditional capacity of the considered AWGN channel under AP and PP constraints on the transmit signal and EH constraints at the EH Rxs. We first prove that the optimal input distribution for the transmit symbols is unique and discrete with a finite number of mass points. In addition, we provide necessary and sufficient conditions for the optimal input distribution. Moreover, we show that if none of the EH Rxs operates in saturation, the R-E tradeoff curve for the problem with multiple EH Rxs can be obtained from the individual R-E curves obtained for each EH Rx separately.

A. Problem Formulation

The discrete-time baseband model for the information channel after down-conversion, matched filtering, and sampling of the continuous-time signal received at the ID Rx is given by $\mathbf{y} = h_l \mathbf{x} + \mathbf{n}$, where $\mathbf{n} \sim \mathcal{N}(0, \sigma_n^2)$ is the Gaussian distributed noise and \mathbf{y} is the information channel output with probability density function (pdf) $p(\mathbf{y})$. We aim at maximizing the average mutual information between \mathbf{x} and \mathbf{y} subject to maximum AP and PP constraints at the transmitter and minimum harvested power constraints at the EH Rxs. In particular, we formulate the problem as

$$\begin{aligned} C &= \sup_{F \in \mathcal{F}_A} I(F) \\ \text{s.t. } C_0 &: \mathbb{E}_F[\mathbf{x}^2] \leq \sigma^2; \\ C_l &: \mathbb{E}_F[P_l(\mathbf{x})] \geq P_{l, \text{req}}, \quad \forall l \in \mathcal{L}, \end{aligned} \quad (18)$$

where \mathcal{F}_A is the set of all input distributions of \mathbf{x} that satisfy the PP constraint $|\mathbf{x}| \leq A$ in (17), i.e., $\forall F \in \mathcal{F}_A, \int_{-A}^A dF(x) = 1$. $I(F)$ is the mutual information between \mathbf{x} and \mathbf{y} achieved by input distribution F and given by $I(F) = \int_{-A}^A i(x; F) dF(x)$, where $i(x; F)$ is the marginal information density defined as $i(x; F) \triangleq \int_{\mathcal{Y}} p(y|x) \log_2 \frac{p(y|x)}{p(y; F)} dy$, $p(y; F)$ is the output pdf assuming input distribution F , and $p(y|x)$ is the output pdf conditioned on the transmission of symbol x [22]. σ^2 is the AP budget, $P_l(x)$ is the harvested power function at the l^{th} EH Rx given in (15), and $P_{l, \text{req}}$ is the minimum required harvested power at EH Rx l . For the purpose of exposition, we define $g_0(F) \triangleq \int_{-A}^A x^2 dF(x) - \sigma^2$

¹¹We assume that the transmitter has perfect knowledge of the circuit parameters of the EH Rxs. The EH Rxs may retransmit these parameters to the transmitter in intervals dictated by variations due to temperature changes and aging.

and $g_l(F) \triangleq P_{l, \text{req}} - \int_{-A}^A P_l(x) dF(x)$, $\forall l \in \mathcal{L}$. Hence, constraints C_0 and $C_l, \forall l \in \mathcal{L}$, can be written as $g_l(F) \leq 0, \forall l \in \{0\} \cup \mathcal{L}$.

B. Properties of the Optimal Input Distribution

In the following, we investigate some important properties of the optimal input distribution.

1) *Uniqueness of the Optimal Input Distribution:* We establish the uniqueness of the optimal input distribution for problem (18) in the following theorem.

Theorem 1. The conditional capacity C in (18) is achieved by a *unique* optimal input distribution function F_0 , i.e., $C = \sup_{F \in \Omega} I(F) = I(F_0)$, where $\Omega \subset \mathcal{F}_A$ is the set of input distributions that satisfy the PP constraint and constraints $C_l, \forall l \in \{0\} \cup \mathcal{L}$, in (18). Furthermore, there exist $\lambda_l \geq 0, \forall l \in \{0\} \cup \mathcal{L}$, such that the conditional capacity C is equivalently given by $C = \sup_{F \in \mathcal{F}_A} I(F) - \sum_{l \in \{0\} \cup \mathcal{L}} \lambda_l g_l(F)$, which is also achieved by F_0 and $\lambda_l g_l(F_0) = 0, \forall l \in \{0\} \cup \mathcal{L}$.

Proof. The proof is provided in Appendix A. ■

2) *Necessary and Sufficient Conditions for the Optimal Input Distribution:* The following theorem provides a necessary and sufficient condition for the optimal input distribution F_0 .

Theorem 2. A necessary and sufficient condition for the input distribution F_0 to achieve the conditional capacity C in (18) is that $\forall F \in \mathcal{F}_A$, there exist $\lambda_l \geq 0, \forall l \in \{0\} \cup \mathcal{L}$, such that

$$\begin{aligned} &\int_{-A}^A \left[i(x; F_0) - \lambda_0 x^2 + \sum_{l \in \mathcal{L}} \lambda_l P_l(x) \right] dF(x) \\ &\leq C - \lambda_0 \sigma^2 + \sum_{l \in \mathcal{L}} \lambda_l P_{l, \text{req}}. \end{aligned} \quad (19)$$

Proof. The proof is provided in Appendix B. ■

Define the points of increase of a distribution function F as those points which have non-zero probability [22]. Next, we provide a more useful condition for characterizing the optimal input distribution.

Corollary 1. Let E_0 be the set of points of increase of a distribution function F_0 on $[-A, A]$, then F_0 is the optimal input distribution of problem (18) if and only if there exist $\lambda_l \geq 0, \forall l \in \{0\} \cup \mathcal{L}$, such that

$$\begin{aligned} s(x) &\triangleq \lambda_0 (x^2 - \sigma^2) - \sum_{l \in \mathcal{L}} \lambda_l (P_l(x) - P_{l, \text{req}}) + C \\ &+ \frac{1}{2} \log_2(2\pi e \sigma_n^2) + \int_{\mathcal{Y}} \frac{e^{-\frac{(y-xh_l)^2}{2\sigma_n^2}}}{\sqrt{2\pi\sigma_n^2}} \log_2(p(y; F_0)) dy \geq 0, \end{aligned} \quad (20)$$

$\forall x \in [-A, A]$, where equality holds if x is a point of increase of F_0 , i.e., if $x \in E_0$.

Proof. The proof is provided in Appendix C. ■

TABLE I: Summary of the main results of the saturation circuit model developed in Section II-B.

Parameter	Expression
Given	$I_s, \eta, V_T, I_{B_v}, B_v, R_s, C_{j0}, R_L, C_L, R_{\text{ant}}, R_{j0} = \eta V_T / I_s, C_j \approx C_{j0}, f_c,$ and P_{in} or \hat{v}_b or \hat{v}_a or x and h_E
Diode I-V characteristic	$i_{d_j}(t) = i_F(t) + i_R(t) = I_s \left(e^{\frac{v_{d_j}(t)}{\eta V_T}} - 1 \right) - I_{B_v} e^{-\frac{B_v}{\eta V_T}} \left(e^{-\frac{v_{d_j}(t)}{\eta V_T}} - 1 \right)$
Rectifier input impedance Z_a	$Z_a(R_d) = R_s + [1/R_d + j\omega_c C_j]^{-1} + [1/R_L + j\omega_c C_L]^{-1}$
Approximations of Z_a	$Z_a _{\text{low power}} \rightarrow Z_a(R_{j0})$ and $Z_a _{\text{high power}} \rightarrow Z_a(R_L/2)$
Bessel function argument β	$\beta = \frac{\hat{v}_a}{\eta V_T} = B \hat{y}_E^{\text{RF}} = B \frac{\hat{v}_b}{\sqrt{R_{\text{ant}}}} = B \sqrt{2P_{\text{in}}} = \sqrt{2} B h_E x$, where $B = [\eta V_T \sqrt{\Re\{1/Z_a^*\}}]^{-1}$
Exact harvested DC power	$P_{\text{out}}(\beta) _{\text{exact}} = \frac{V_{\text{out}}^2(\beta)}{R_L}$, where $V_{\text{out}}(\beta)$ is the solution of $I_s \left[e^{-\frac{V_{\text{out}}(\beta)}{\eta V_T}} \left(1 + \frac{R_s}{R_L} \right) I_0(\beta) - 1 \right] - I_{B_v} e^{-\frac{B_v}{\eta V_T}} \left[e^{\frac{V_{\text{out}}(\beta)}{\eta V_T}} \left(1 + \frac{R_s}{R_L} \right) I_0(\beta) - 1 \right] = \frac{V_{\text{out}}(\beta)}{R_L}$
Approximate harvested DC power	$P_{\text{out}}(\beta) _{\text{approx.}} = \min \left(\left[\frac{1}{a} W_0(ae^a I_0(\beta)) - 1 \right]^2 I_s^2 R_L, \frac{B_v^2}{4R_L} \right)$, where $a = \frac{I_s(R_L + R_s)}{\eta V_T}$.
RF input power at $P_{\text{out}} = \frac{B_v^2}{4R_L}$	$P_{\text{in,sat}} = \frac{1}{2} (\eta V_T \beta_{\text{sat}})^2 \Re \left\{ \frac{1}{Z_a^*(R_{j0})} \right\}$, where β_{sat} is the solution of $I_0(\beta_{\text{sat}}) = e^{\frac{a B_v}{2 I_s R_L}} \left(1 + \frac{B_v}{2 I_s R_L} \right)$.

3) *Discreteness of the Optimal Input Distribution:* The discreteness of the optimal input distribution F_0 for problem (18) is formally stated in the following theorem.

Theorem 3. The optimal input distribution that achieves the conditional capacity in (18) is discrete with a finite number of mass points.

Proof. The proof is provided in Appendix D. ■

C. The Activeness of Only One EH Constraint in (18) for $A < A_{\text{sat}}$

In this section, we consider the case when the transmit amplitude is set to $A < A_{\text{sat}}$ to avoid the saturation of the harvested DC power at the EH Rxs. We prove that, in this case, at the optimal solution, at most one of the EH constraints of problem (18) is active. We note that, owing to the random deployment of the EH Rxs, their channel gains are different with probability one. Moreover, each EH Rx sets its minimum DC power requirement independently. As a result, the solution of problem (18) with only EH constraint C_l is different from that with only EH constraint $C_{l'}, \forall l \neq l' \in \mathcal{L}$.

Lemma 1. *Considering the harvested power model in (15), in the unsaturated case, i.e., for $A < A_{\text{sat}}$, if an input distribution $F_L(x) \in \mathcal{F}_A$ provides a larger average harvested power than another distribution $F_s(x) \in \mathcal{F}_A$, for one EH Rx, then $F_L(x)$ also provides larger average harvested powers than $F_s(x)$, for all other EH Rxs. That is, if for some l , $\mathbb{E}_{F_L}[P_l(x)] > \mathbb{E}_{F_s}[P_l(x)]$, then $\mathbb{E}_{F_L}[P_l(x)] > \mathbb{E}_{F_s}[P_l(x)], \forall l \in \mathcal{L}$.*

Proof. Lemma 1 follows since the harvested power function in (15) for $A < A_{\text{sat}}$ is monotonically increasing for $0 < x < A, \forall$ EH Rxs, since the Bessel function $I_0(\cdot)$, the LambertW function $W_0(\cdot)$, and the quadratic function are all monotonically increasing for $x > 0$. Similarly, the harvested power function in (15) is monotonically increasing in the channel gain h_{E_l} . That is, if $h_{E_1} > h_{E_2}$, then $P_1(x) > P_2(x), \forall 0 < x < A$. Hence, if the integration of one $P_l(x)$ with respect to some distribution $F_L(x) \in \mathcal{F}_A$ is larger than with respect to distribution

$F_s(x) \in \mathcal{F}_A$, i.e., $\int_0^A P_l(x) dF_L(x) > \int_0^A P_l(x) dF_s(x)$, then this relation must also hold for any other EH Rx l' , i.e., $\int_0^A P_{l'}(x) dF_L(x) > \int_0^A P_{l'}(x) dF_s(x), \forall l' \neq l \in \mathcal{L}$. ■

Theorem 4. In problem (18), for $A < A_{\text{sat}}$, at most one EH constraint is active. In particular, the active EH constraint is the one, which when all other EH constraints are removed, results in the smallest achievable rate at the ID Rx, denoted by $I(F_0)$.

Proof. The proof is provided in Appendix E. ■

The R-E tradeoff curve associated with problem (18) is an $(L+1)$ -dimensional curve formed by the points $(I(F_0), \mathbb{E}_{F_0}[P_1(x)], \dots, \mathbb{E}_{F_0}[P_L(x)])$ obtained by solving (18) for all combinations of feasible minimum required DC powers $P_{l,\text{req}}, l \in \mathcal{L}$, at the EH Rxs. Owing to Theorem 4, for $A < A_{\text{sat}}$, this $(L+1)$ -dimensional R-E curve can be obtained from the L two-dimensional R-E curves of the individual EH Rxs, where the individual R-E curve of EH Rx l is obtained by solving problem (18) with the AP and PP constraints and only EH constraint C_l for different required DC powers $P_{l,\text{req}}$. In particular, assuming K required DC powers for each EH Rx, problem (18) has to be solved only KL times to determine the corresponding $(L+1)$ -dimensional R-E curve instead of K^L times.

Remark 3. The results in this section hold only for $A < A_{\text{sat}}$. If $A \geq A_{\text{sat}}$, then some EH Rxs may operate in saturation. In particular, let $A \geq A_{T,\text{sat}_l}, \forall l \in \mathcal{L}_{\text{sat}}$ and $A < A_{T,\text{sat}_l}, \forall l \in \mathcal{L}_{\text{non-sat}}$, then according to Theorem 4, at most one EH constraint of the EH Rxs in set $\mathcal{L}_{\text{non-sat}}$ may be active. However, in addition, also more than one EH constraint for the EH Rxs in set \mathcal{L}_{sat} may be active. This is because, when $A \geq A_{\text{sat}}$ holds, Lemma 1 does not hold since $P_l(x)$ is not monotonically increasing in $0 < x < A$ for $l \in \mathcal{L}_{\text{sat}}$. For example, it will be shown in Section IV-B that the optimal input distribution that maximizes the average harvested power is different for the EH Rxs in set \mathcal{L}_{sat} . Hence, an input distribution that provides more energy for one EH Rx in set \mathcal{L}_{sat} may

provide less energy for another EH Rx in set \mathcal{L}_{sat} .

Having established the properties of the optimal solution for problem (18), we aim next at getting more insights into the optimal distribution by studying special cases and generalizations of problem (18).

IV. SPECIAL CASES AND GENERALIZATIONS

In this section, we study the special cases of maximum WIT and maximum WPT systems to obtain further insight. Based on these extreme cases, we propose a sub-optimal but insightful distribution which bridges the gap between the two systems. Then, we generalize problem (18) to the complex domain.

A. Maximum Information Transfer

The maximum information transfer rate can be obtained by dropping all L EH constraints in (18). In this case, the problem reduces to the capacity of an AP and PP constrained AWGN channel, which was solved by Smith in [22], who proved that the optimal input distribution, denoted by F_0^{WIT} , is discrete with a finite number of mass points. In addition, he showed that F_0^{WIT} cannot be expressed in closed form but can be obtained numerically resulting in a maximum achievable information rate of $C_{\max} \triangleq I(F_0^{\text{WIT}})$. With this solution, the average harvested power at the l^{th} EH Rx is $P_{l,\min} \triangleq \mathbb{E}_{F_0^{\text{WIT}}}[P_l(\mathbf{x})]$. Hence, in problem (18), if $P_{l,\text{req}} \leq P_{l,\min}$, $\forall l \in \mathcal{L}$, holds, the harvested power $P_{l,\min}$ is attained at the EH Rx's without compromising the maximum information rate at the ID Rx¹². Furthermore, if additionally the PP constraint is relaxed, i.e., $A \rightarrow \infty$, problem (18) reduces to the maximization of the mutual information of the AP constrained AWGN channel. For this special case, the optimal input distribution is known to be the *continuous* zero-mean Gaussian distribution given by $\frac{1}{\sqrt{2\pi\sigma^2}}e^{-x^2/(2\sigma^2)}$ [21], cf. Case 1 in Appendix D for $A \rightarrow \infty$, and the maximum achievable rate is the well-known Shannon capacity given by $\frac{1}{2} \log_2 \left(1 + \frac{\sigma^2 h_l^2}{\sigma_n^2}\right)$.

B. Maximum Energy Transfer

In this section, we formulate the maximum WPT problem for EH Rx l in (21) and obtain the optimal input distribution and the maximum average harvested power in closed form in Theorem 5. In particular,

$$P_{l,\max} = \sup_{F \in \mathcal{F}_A} \mathbb{E}_F [P_l(\mathbf{x})] \\ \text{s.t. } C_0 : \mathbb{E}_F [\mathbf{x}^2] \leq \sigma^2. \quad (21)$$

Theorem 5. Define $A'_l \triangleq \min(A, A_{T,\text{sat}_l})$ with A_{T,sat_l} as defined in Section II-C. Then, the optimal distribution obtained from problem (21) has a probability mass function given by

$$dF_0^{\text{WPT}}(x, A'_l) = \begin{cases} p & x = -A'_l \\ [1 - (p+q)]^+ & x = 0 \\ q & x = A'_l \end{cases}. \quad (22)$$

¹²If however, $\exists l$ such that $P_{l,\text{req}} > P_{l,\min}$, then the achievable information rate has to be compromised, i.e., $I(F_0) < C_{\max}$, in order for the l^{th} EH Rx to be able to harvest enough energy.

where $p, q \geq 0$ and $p+q = \min\{\sigma^2/A_l'^2, 1\}$. The maximum average harvested power at EH Rx l is

$$P_{l,\max}(A'_l) = \mathbb{E}_{F_0^{\text{WPT}}} [P_l(\mathbf{x})] = \begin{cases} \frac{\sigma^2}{A_l'^2} P_l(A'_l) & \frac{\sigma^2}{A_l'^2} < 1 \\ P_l(A'_l) & \frac{\sigma^2}{A_l'^2} > 1 \end{cases}, \quad (23)$$

where $l \in \mathcal{L}$ and the average mutual information at the ID Rx is $I(F_0^{\text{WPT}}) = \int i(x; F_0^{\text{WPT}}) dF_0^{\text{WPT}}(x)$.

Proof. The proof is provided in Appendix F. ■

Remark 4. Theorem 5 indicates that for $A < A_{T,\text{sat}_l}$, the larger the peak amplitude A in problem (21) is, the higher the maximum average power harvested by EH Rx l given in (23), since $P_l(x)$ and $P_l(x)/x^2$ increase monotonically for $0 < x \leq A$ as shown in the proof of Lemma 1 and in Appendix F, respectively. However, increasing the peak amplitude A beyond A_{T,sat_l} has no effect on the maximum average harvested power, which saturates to an asymptotic value of $P_{l,\max}(A_{T,\text{sat}_l})$, $\forall A \geq A_{T,\text{sat}_l}$, cf. (23), and the optimal input distribution for maximum WPT in (22) saturates to the asymptotic on-off distribution $dF_0^{\text{WPT}}(x, A_{T,\text{sat}_l})$. This asymptotic behaviour is confirmed by the numerical results provided in Section V, cf. Fig. 7. We also note that from the WPT perspective, the specific values of p and q in (22) are irrelevant as long as they satisfy $p+q = \min\{\sigma^2/A_l'^2, 1\}$. For WIT, the rate is maximized when $p=q=\min\{\sigma^2/(2A_l'^2), 1/2\}$.

Remark 5. For the linear EH model, $P_l(x)/x^2$ is constant $\forall x$. From (35) in Appendix F, any distribution satisfying the AP and PP constraints maximizes the harvested energy. Consequently, the optimal distribution for maximum WIT is also optimal for maximum WPT. Hence, for an AWGN channel with the linear EH model, a tradeoff between WIT and WPT does not exist. This result was stated in [2, p. 5].

C. Proposed Suboptimal Distribution

Motivated by studying the extreme cases of WIT and WPT, we propose a suboptimal distribution for problem (18) with one EH Rx l . This distribution superimposes a truncated Gaussian distribution with mass points at $-A'_l$ and A'_l , i.e.,

$$f_s(x) = \begin{cases} b e^{-dx^2} + c [\delta(x+A'_l) + \delta(x-A'_l)], & -A'_l \leq x \leq A'_l \\ 0, & \text{otherwise,} \end{cases} \quad (24)$$

where b and c are obtained to satisfy the AP constraint and the unit area condition of the pdf $f_s(x)$. In particular, $b = \frac{1-2c}{\sqrt{\frac{\pi}{d}} \text{erf}(\sqrt{d}A'_l)}$ and $c \leq \left(\sigma_x^2 - \frac{1}{2d} + \frac{A'_l \exp(-dA_l'^2)}{\sqrt{\pi} \text{erf}(\sqrt{d}A'_l)}\right) / \left(2A_l'^2 - \frac{1}{d} + \frac{2A'_l \exp(-dA_l'^2)}{\sqrt{\pi} \text{erf}(\sqrt{d}A'_l)}\right)$, where $\text{erf}(x) = \frac{1}{\sqrt{\pi}} \int_{-x}^x \exp(-t^2) dt$ is the error function and d is a design parameter with which the harvested power increases. Since (24) superimposes the optimal distributions for WIT and WPT, it is expected to provide a close-to-optimal R-E tradeoff performance. This is confirmed by numerical evaluations in Section V-B.

D. Complex Signaling

In this section, we extend problem (18) to the complex domain. In particular, the transmit signal $x(t) = \sum_{k=-\infty}^{\infty} x[k]g(t-kT)$ is composed of complex-valued symbols $x[k] \triangleq r[k]e^{j\theta[k]}$, where $r[k]$ and $\theta[k]$ are the amplitude and phase of the transmit symbol $x[k]$, respectively. The channel fading gains for the ID and EH Rxs are also complex-valued given by $h_I = |h_I|e^{j\phi_I}$ and $h_{E_l} = |h_{E_l}|e^{j\phi_{E_l}}$, respectively. Hence, assuming a rectangular pulse, the received signal at the EH Rx is given by $y_{E_l}(t) = r[k]|h_{E_l}|e^{j(\theta[k]+\phi_{E_l})}$ and $y_{E_l}^{\text{RF}}(t) = \sqrt{2}r[k]|h_{E_l}|\cos(2\pi f_c t + \theta[k] + \phi_{E_l})$, $kT - T/2 < t \leq kT + T/2$, in the equivalent complex baseband and RF domains, respectively. Let \mathbf{r} and $\boldsymbol{\theta}$ be the random variables, whose realizations in time slot k are $r[k]$ and $\theta[k]$, respectively, i.e., $\mathbf{x} = \mathbf{r}e^{j\boldsymbol{\theta}}$. Hence, from Section II-B, the integral involved in the forward current in the first term on the LHS of (4) for EH Rx l reduces to $I_0(\beta) = \frac{1}{T} \int_T e^{\frac{v_a(t)}{\eta V_T}} dt = \frac{1}{T} \int_T e^{B y_{E_l}^{\text{RF}}(t)} dt = \frac{1}{T} \int_T e^{\sqrt{2}B|h_{E_l}|\mathbf{r} \cos(2\pi f_c t + \theta + \phi_{E_l})} dt = I_0(\sqrt{2}B|h_{E_l}|\mathbf{r})$. This indicates that the power harvested at the EH Rx does not depend on the phase of the received signal. Hence, similar to (15), with complex signaling, the harvested power at the l^{th} EH Rx can be approximated by $P_l(r) \triangleq P_{\text{out}}(\sqrt{2}B|h_{E_l}|\mathbf{r}) \Big|_{\text{approx.}} = \min \left(\left[\frac{1}{a} W_0(ae^a I_0(\sqrt{2}B|h_{E_l}|\mathbf{r})) - 1 \right]^2 I_s^2 R_L, \frac{B_v^2}{4R_L} \right)$, and the AP constraint in (18) can be written as $\mathbb{E}[\mathbf{r}^2] \leq \sigma^2$. At the ID Rx, the baseband transmission model $\mathbf{y} = \mathbf{x}h_I + \mathbf{n}$ can be written in polar coordinates as $\mathbf{R}e^{j\psi} = |h_I|\mathbf{r}e^{j(\theta+\phi_I)} + \mathbf{n}$, where \mathbf{R} and ψ are random variables representing the amplitude and phase of the received signal \mathbf{y} and $\mathbf{n} \sim \mathcal{CN}(0, 2\sigma_n^2)$.

Lemma 2. The optimal distribution of transmit signal $\mathbf{x} = \mathbf{r}e^{j\boldsymbol{\theta}}$ for problem (18) in the complex domain is characterized by mutually independent amplitude \mathbf{r} and phase $\boldsymbol{\theta}$, and a uniformly distributed phase $\boldsymbol{\theta}$.

Proof. The proof is provided in Appendix G. ■

Hence, with complex signalling, the conditional capacity problem in (18) reduces to finding the optimal distribution F_r of the amplitude of the transmit signal based on the following optimization problem

$$\begin{aligned} C &= \sup_{F_r \in \mathcal{F}_A} I(F_r) \\ \text{s.t. } C_0 &: \mathbb{E}_{F_r}[\mathbf{r}^2] \leq \sigma^2; \\ C_l &: \mathbb{E}_{F_r}[P_l(\mathbf{r})] \geq P_{l,\text{req}}, \forall l \in \mathcal{L}. \end{aligned} \quad (25)$$

Next, we investigate the properties of the optimal input amplitude distribution in the following theorem.

Theorem 6. The optimal input amplitude distribution of problem (25) is unique and discrete with finite number of mass points. Furthermore, if E_0 is the set of points of increase of a distribution function F_{r_0} on $[0, A]$, then F_{r_0} is the optimal input distribution if and only if there

exist $\lambda_l \geq 0$, $\forall l \in \{0\} \cup \mathcal{L}$, such that

$$\begin{aligned} s(r) &\triangleq \lambda_0(r^2 - \sigma^2) - \sum_{l \in \mathcal{L}} \lambda_l(P_l(r) - P_{l,\text{req}}) + C + \log_2(e\sigma_n^2) \\ &+ \int \frac{R}{\sigma_n^2} e^{-\frac{R^2 + r^2 |h_I|^2}{2\sigma_n^2}} I_0\left(\frac{Rr|h_I|}{\sigma_n^2}\right) \log_2\left(\frac{f_R(R; F_{r_0})}{R}\right) dR \geq 0, \end{aligned} \quad (26)$$

$\forall r \in [0, A]$, where equality holds if r is a point of increase of F_{r_0} , i.e., if $r \in E_0$.

Proof. The proof is provided in Appendix H. ■

V. NUMERICAL RESULTS

In this section, we first validate the accuracy of the derived harvested DC power functions in (6) and (14) via circuit simulations. Afterwards, we evaluate the solutions for problems (18) and (25) for real and complex AWGN channels, respectively, under AP, PP, and EH constraints. The channel gains are given by $|h_k|^2 = (v/(4\pi d_k f_c))^\alpha$ for $k \in \{I, E_l\}$, where v is the speed of light, α is the path loss exponent, d_I and d_{E_l} are the distances between the transmitter and the ID and the l^{th} EH Rx, respectively. Table II summarizes the parameters adopted in the numerical results.

A. ADS Circuit Simulation and Validation of the Harvested DC Power Function $P(x)$ in Table I

In this section, we validate the harvested DC power function given in Table I through circuit simulations on ADS [33], as shown in Fig. 3. In particular, we use the SMS7630 Schottky diode, since it operates at very low input RF powers¹³ and does not need external bias [32]. An LC matching network is fine-tuned for every input power to provide perfect matching (reflection coefficient < -50 dB). For example, at $P_{\text{in}} = -24$ dBm, the matching network elements are $L = 15.98$ nH and $C = 0.1376$ pF, cf. Fig. 3. The remaining circuit parameters are as in Table II. Fig. 4 shows a very good match between the harvested DC power obtained from the circuit simulations and the analytical expressions from Table I.

B. Numerical Evaluation of the Conditional Capacity Problems (18) and (25)

Although we showed in Sections III-B3 and IV-D that the optimal input distribution is discrete with a finite number of mass points, the number and positions of the mass points are not known. However, since problems (18) and (25) are convex $\forall F \in \mathcal{F}_A$, they can be solved numerically using CVX [34] by discretizing the interval $x = [-A, A]$ with a sufficiently small step size, i.e., $\Delta x \rightarrow 0$ and the interval $r = [0, A]$ with $\Delta r \rightarrow 0$, to obtain the symbol set. Then, for this symbol set, the harvested power functions $P_l(x)$ in (15) and $P_l(r)$ in Section IV-D are calculated and used in the EH constraints in

¹³In the SMS7630 Schottky diode's data sheet [32], the diode detector circuit shown in [32, Fig. 2], which is similar to the one considered in this paper, is functional for RF input powers as low as -40 dBm as is evident from the measured output voltage shown in [32, Fig. 7].

TABLE II: Numerical parameters.

Parameter	Value
Carrier frequency	$f_c = 2.45$ GHz
Path loss exponent	$\alpha = 2.5$
Noise power at the EH Rxs	$\sigma_n^2 = -80$ dBm in Figs. 5-8 and $\sigma_n^2 = -50$ dBm per signal dimension in Figs. 9, 10.
Distance between transmitter and ID Rx	$d_I = 25$ m
Distance between transmitter and EH Rxs	In Figs. 5-8, one EH Rx at $d_{E1} = 5$ m. In Figs. 9, 10, three EH Rxs at distances $d_{E1} = 3$ m, $d_{E2} = 3.5$ m, and $d_{E3} = 4$ m
Circuit parameters, cf. Fig. 2	$R_{ant} = 50 \Omega$, $R_L = 10$ k Ω , $C_L = 1$ nF
SMS7630 Schottky diode parameters [32]	$I_s = 5 \mu A$, $R_s = 20 \Omega$, $\eta = 1.05$, $C_{j0} = 0.14$ pF, $I_{Bv} = 100 \mu A$, and $B_v = 2$ V.

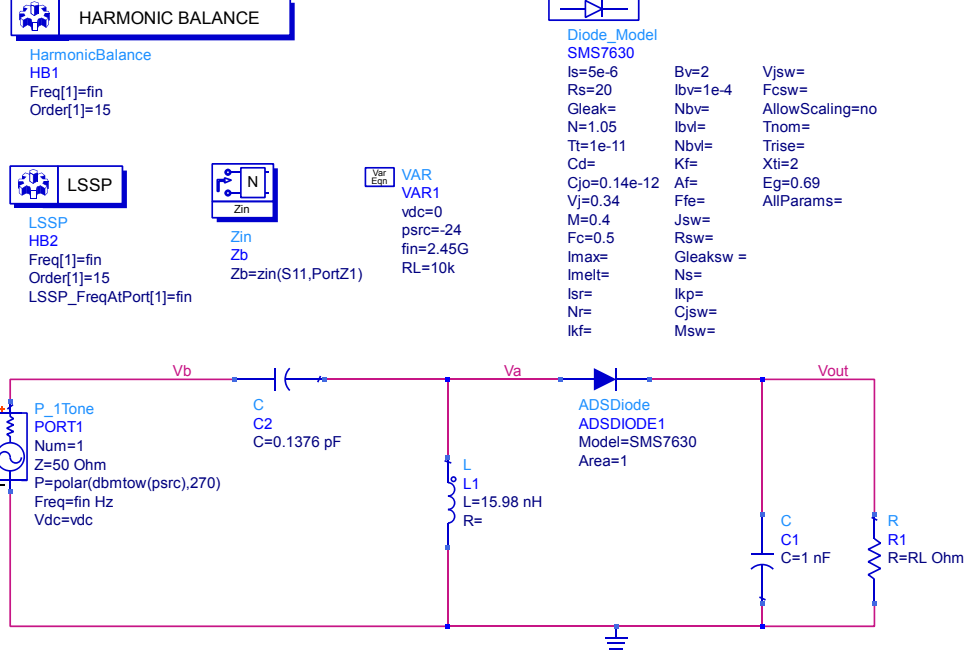


Fig. 3: ADS schematic of the rectenna circuit model in Fig. 2.

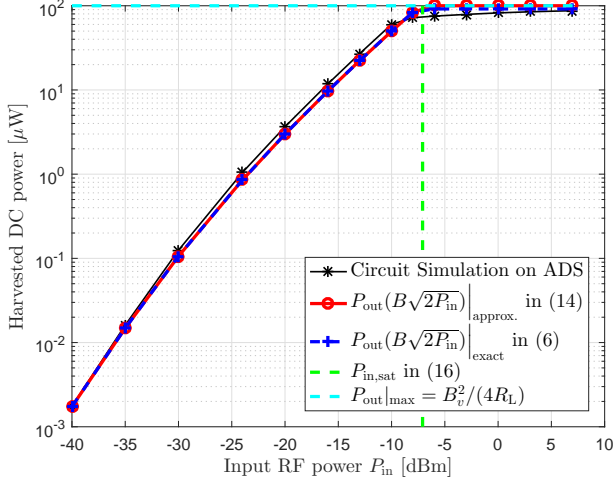


Fig. 4: Harvested DC power vs. input RF power: ADS circuit simulation and analytical results from Table I.

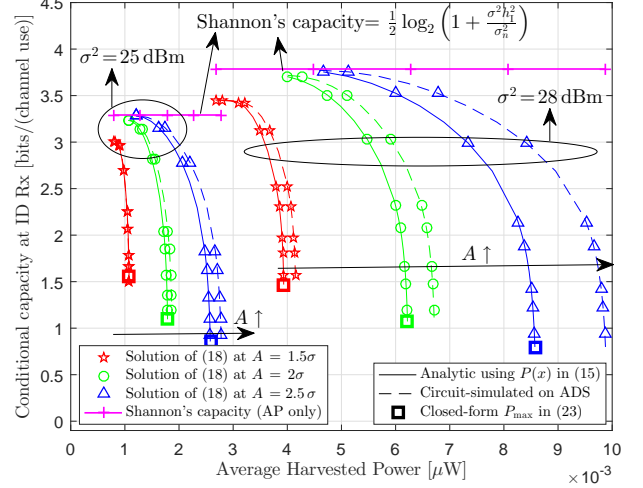


Fig. 5: R-E regions for different AP and PP constraints.

CVX. The optimality of the numerically obtained input distribution can be checked by verifying the necessary and sufficient conditions in Corollary 1 for real signaling and in Theorem 6 for complex signaling.

In Figs. 5-8, we consider a real-valued AWGN channel and a SWIPT system with one ID Rx and only one EH Rx located at $d_{E1} = 5$ m, i.e., with $A_{T,sat_1} =$

$\sqrt{P_{in,sat}}/|h_{E1}| = 33.28 \text{ V} = 23.56 \sigma$. Except for Fig. 7, all peak amplitudes A in Figs. 5-8 are less than A_{T,sat_1} to avoid driving the rectifier into saturation.

In Fig. 5, we plot the R-E curves of the considered system for different AP and PP constraints. In particular, we obtain each R-E curve by solving problem (18) for different required harvested powers P_{req} . The optimal input distribution $F_0(x)$ is then

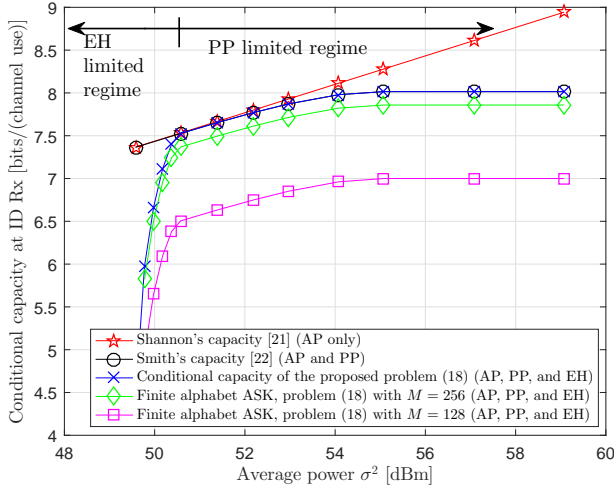


Fig. 6: Conditional capacity of problem (18) and achievable rate for different finite alphabets with $A = 30.75$ V and $P_{\text{req}} = 7.5$ μ W.

used to obtain the conditional capacity at the ID Rx, $I(F_0)$, and the average harvested power at the EH Rx, $\mathbb{E}_{F_0}[P_1(\mathbf{x})] = \int_{-A}^A P_1(x) dF_0(x)$, with $P_1(x)$ in (15). In addition, we plot the circuit-simulated average harvested power $\mathbb{E}[P_{\text{ct}}(\mathbf{x})] = \int_{-A}^A P_{\text{ct}}(x) dF_0(x)$, where $P_{\text{ct}}(x) = P_{\text{ct}}(P_{\text{in}} = (xh_E)^2)$ is the power function shown in Fig. 4 obtained by interpolating the circuit-simulated data from ADS. In Fig. 5, it is observed that the circuit-based average harvested DC power is slightly higher than the analytical one. This is because, as shown in Fig. 4, the circuit-simulated harvested power function lies slightly above the analytical one. Moreover, Fig. 5 reveals that unlike for the linear EH model [2], for the considered nonlinear EH model, there exists a non-trivial tradeoff between the information rate transmitted to the ID Rx and the power delivered to the EH Rx. In fact, for a larger required average DC power, the optimal input distribution forces the transmitter to transmit more often with the peak amplitudes $x = \pm A$ and less often in the range $x \in (-A, A)$. This leads to higher average harvested power for the EH Rx at the expense of a lower information rate at the ID Rx. Moreover, the maximum feasible average harvested DC power, obtained by solving problem (21), matches the closed-form expression in (23). Furthermore, it can be observed that the higher the peak-amplitude A , the larger the achieved R-E region. In deed, for a larger peak amplitude, the transmitter has to transmit less often with the peak amplitudes to achieve the same average harvested power and can more often choose $x \in (-A, A)$, allowing for a higher information rate at the ID Rx. Moreover, as A increases, the maximum possible average harvested power increases, as given in (23) for $A < A_{T,\text{sat}_1}$.

In Fig. 6, we plot the conditional capacity of problem (18) as a function of the AP constraint σ^2 for a required DC power of 7.5 μ W. The peak amplitude constraint is set to $A = 30.75$ V, which results in a received RF peak power of $(Ah_{E1})^2 \equiv -8$ dBm, i.e., the rectifier is not driven into saturation, cf. Fig. 4. Fig. 6 reveals that, for low APs, the system is EH-limited. In particular, compared to Smith's problem in [22] with AP and PP constraints, the EH

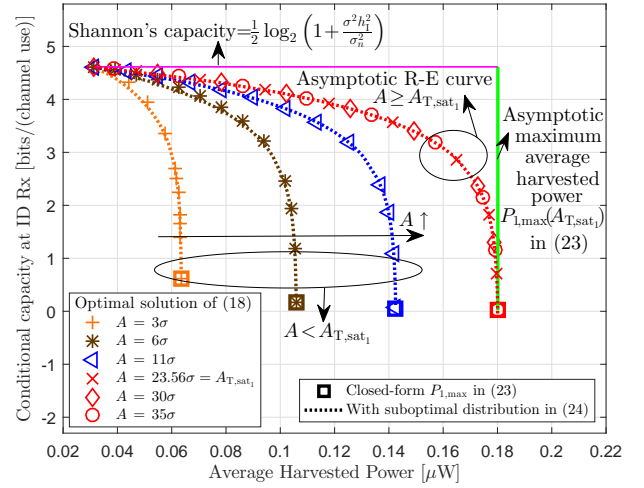


Fig. 7: R-E curves for optimal distribution from (18) and suboptimal distribution from (24) for $\sigma^2 = 33$ dBm.

constraint imposed in problem (18) incurs a capacity loss which decreases with the AP. On the other hand, for large APs, the system is PP limited. That is, the EH constraint is inactive and the conditional capacity of our problem coincides with Smith's capacity in [22]. In addition, we plot the maximum information rate for amplitude shift keying (ASK), which is obtained by solving problem (18) for M symbols at $x = \frac{2Ak}{M-1} - A$, $k = 0, 1, \dots, M-1$. The larger the alphabet size, the closer the rate achieved by the finite alphabet is to that achieved by the optimal input distribution. Moreover, in the PP-limited regime, the capacities of all PP-constrained schemes saturate for high APs.

In Fig. 7, we show the R-E curves obtained for the optimal solution of problem (18) and the suboptimal distribution given in (24), respectively. The AP constraint is set to $\sigma^2 = 33$ dBm and different values of the PP constraint are considered. It is observed that the R-E curves for the suboptimal distribution are very close to the optimal ones. This behaviour is expected since the suboptimal distribution is a weighted sum of the optimal distribution for maximum WIT with $A \rightarrow \infty$ and the optimal distribution for maximum WPT, cf. Sections IV-A to IV-C. Moreover, interestingly, it is observed that all R-E curves for peak amplitudes $A \geq A_{T,\text{sat}_1}$ are identical. This is because $\forall A \geq A_{T,\text{sat}_1}$, the optimal input distribution for maximum WPT saturates at the asymptotic on-off distribution $dF_0^{\text{WPT}}(x, A_{T,\text{sat}_1})$ in (22) and the corresponding maximum average harvested power saturates at $P_{1,\text{max}}(A_{T,\text{sat}_1})$ in (23). At the same time, since $A_{T,\text{sat}_1} = 23.56\sigma$ is large compared to σ , $\forall A \geq A_{T,\text{sat}_1}$ the optimal input distribution for maximum WIT converges to that for $A \rightarrow \infty$, namely to the asymptotic zero-mean Gaussian distribution. Hence, the optimal distribution that maximizes the R-E region also converges to an asymptotic distribution (very close to the suboptimal distribution in (24) with $A'_1 = A_{T,\text{sat}_1}$), which yields the asymptotic R-E curve shown in red in Fig. 7.

In Fig. 8, we assume an AP constraint of $\sigma^2 = 33$ dBm and a peak amplitude constraint of $A = 3\sigma$. We plot the numerically-obtained optimal distributions for (a) the

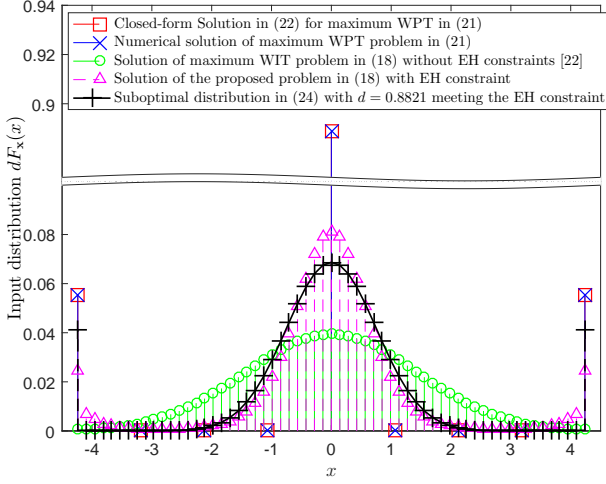


Fig. 8: Numerically-obtained and closed-form input distributions for the SWIPT problem in (18) and the maximum WPT solution for $\sigma^2 = 33$ dBm, $A = 3\sigma$, and $P_{\text{req}} = 0.047 \mu\text{W}$.

maximum WIT problem [22], which has the shape of a truncated Gaussian distribution (b) the maximum WPT problem in (21), which perfectly matches the closed-form optimal distribution in (22) with mass points at 0 and $\pm A$, and (c) the SWIPT problem in (18), whose envelope is close to a truncated Gaussian with additional mass points at $\pm A$. This explains why in Fig. 7, the suboptimal distribution in (24) leads to a close-to-optimal R-E performance.

In Figs. 9 and 10, we consider complex-valued transmission and solve problem (25) for an AP of $\sigma^2 = 43$ dBm and a peak amplitude of $A = 3\sigma = 13.4$ V. We consider a system with one ID Rx at $d_1 = 25$ m and three EH Rxs at $d_{E1} = 3$ m, $d_{E2} = 3.5$ m, and $d_{E3} = 4$ m, i.e., with $A_{T,\text{sat}1} = 18$ V, $A_{T,\text{sat}2} = 21.8$ V, and $A_{T,\text{sat}3} = 25.8$ V, respectively. Hence, $A < A_{\text{sat}}$ and the results in Theorem 4 hold. In Fig. 9, we first consider the case when only one EH Rx requires a certain amount of DC power, while the other two EH Rxs have no power demands and they passively harvest from the received power. In this case, the EH constraint of only the power-demanding EH Rx is present in (25) and the corresponding individual R-E curves are plotted in Fig. 9. It can be observed that the closer the EH Rx is to the transmitter, the larger the R-E region gets. Furthermore, at low required DC powers, the EH constraint of the power-demanding EH Rx is inactive and the individual R-E curves converge to the capacity of the complex AWGN channel with AP and PP constraints only, as obtained in [23]. For the considered low AP constraint, this limiting capacity practically coincides with Shannon's capacity given by $\log_2 \left(1 + \frac{\sigma^2 |h_1|^2}{2\sigma_n^2} \right) = 2$ bits/(channel use).

Next, we consider the case when all three EH Rxs require a certain DC power, given by $P_{l,\text{req}}^*$, $l = 1, 2, 3$, as shown in Fig. 9 by the projection of the star markers “ \star ” onto the x-axis. According to Theorem 4, the only active EH constraint, is that of the EH Rx for which the ID Rx rate of its individual R-E curve is the smallest. In the considered example, the EH constraint of EH Rx 2 is the only active one and the conditional capacity at the

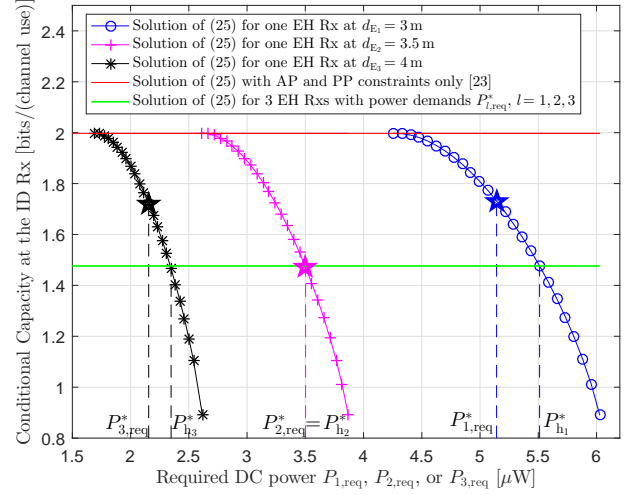


Fig. 9: Individual R-E curves for three EH Rxs for $\sigma^2 = 43$ dBm, $A = 3\sigma$. The star markers represent the intersection between the individual required DC powers with the individual R-E curves.

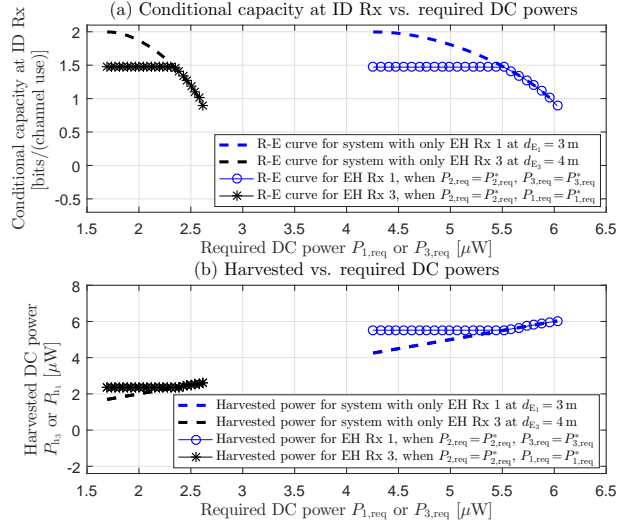


Fig. 10: R-E curves and average harvested DC powers for $\sigma^2 = 43$ dBm, $A = 3\sigma$ using the required DC powers with star markers in Fig. 9 for two EH Rxs and varying the required DC power of only one EH Rx (1 or 3).

ID Rx is 1.47 bits/(channel use). Furthermore, the actual harvested DC powers at the EH Rxs, denoted by P_{h1}^* , $l = 1, 2, 3$, are the DC power values of the points obtained by the intersection of the individual R-E curves with the horizontal line of the conditional capacity of the ID Rx. Only the active EH Rx harvests as much as it requires, while the inactive ones harvest more power than required, i.e., $P_{h1}^* > P_{1,\text{req}}^*$, $P_{h2}^* = P_{2,\text{req}}^*$, and $P_{h3}^* > P_{3,\text{req}}^*$, as shown in Fig. 9.

To shed further light on the behaviour of the SWIPT system with multiple EH Rxs, in Fig. 10, we sweep the required DC power of either EH Rx 1 or 3, respectively, and fix the required DC powers of the other two EH Rxs to the values given by the star markers “ \star ” in Fig. 9, namely, $P_{2,\text{req}}^*$ and $P_{l,\text{req}}^*$, $l = 3, 1$. Then, we plot the conditional capacity achieved at the ID Rx as well as the harvested powers at EH Rx $l \in \{1, 3\}$. As can be observed, for all required DC powers $P_{l,\text{req}} < P_{h1}^*$, the EH constraint of EH Rx 2 is the only active EH constraint and the conditional capacity at the ID Rx is fixed, whereas the

harvested DC power at user l is $P_{h_l}^*$. On the other hand, when $P_{l,\text{req}} > P_{h_l}^*$, EH Rx l provides the only active EH constraint and the conditional capacity of the ID Rx is determined by the individual R-E curve of EH Rx l , as shown in Fig. 10(a). Moreover, EH Rx l harvests as much as it requires, i.e., $P_{h_l} = P_{l,\text{req}}$.

VI. CONCLUSION

We studied the conditional capacities of real- and complex-valued SWIPT systems with separated ID and EH Rxs under AP, PP, and EH constraints. We developed a novel circuit-based nonlinear EH model that accounts for the saturation of the harvested DC powers at high input RF powers. The accuracy of this model was verified with circuit simulations. Our results reveal that, for a given AP constraint, the R-E tradeoff curve saturates for high PP constraints due to the saturation of the harvested DC power. We proved that the optimal input distribution that maximizes the R-E region is discrete with a finite number of mass points. Moreover, the optimal input distribution for maximum WPT was found to be an on-off distribution. We proposed a suboptimal distribution, which superimposes the optimal distributions for WPT and WIT and showed that its R-E performance closely approaches the optimal one. Future work may include extensions to multisine signals, fading channels, and co-located EH and ID Rxs.

APPENDIX A – PROOF OF THEOREM 1

We first prove the existence of a unique distribution $F_0 \in \Omega$ that maximizes the mutual information $I(F)$. It suffices to show that the optimization problem in (18) is convex, i.e., that the set Ω is convex and compact in some topology and that $I(F)$ is continuous and strictly concave in F . The convexity of the set Ω follows from the convexity of the set of distribution functions \mathcal{F}_A (defined by $\int_{-A}^A dF(x) = 1$) and the linearity of the AP and EH constraints in F . Hence, constraints $g_l(F) \leq 0$, $\forall l \in \{0\} \cup \mathcal{L}$, are convex. The proof of the compactness of Ω is similar to that in [25, Appendix I.A]. Next, we show that the mutual information is continuous and strictly concave in F . The mutual information resulting from an input distribution F is $I(F) = h_{\mathbf{y}}(F) - h_N$, where $h_{\mathbf{y}}(F)$ is the entropy of output \mathbf{y} assuming an input distribution F , and h_N is the noise entropy given by $h_N = \frac{1}{2} \log_2(2\pi e \sigma_n^2)$. Since h_N is constant, it suffices to show that $h_{\mathbf{y}}(F)$ is continuous and strictly concave. The proof of the continuity of $h_{\mathbf{y}}(F)$ is given in [25, Appendix I.B]. Next, we show that the entropy function $h_{\mathbf{y}}(F)$ is strictly concave in F . Since $h_{\mathbf{y}}(F) = -\int_{-\infty}^{\infty} p(y; F) \log_2(p(y; F)) dy$ is a strictly concave function of the output pdf $p(y; F)$ and $p(y; F) = \int_{-\infty}^{\infty} p(y|x) dF(x)$ is a linear function in F , it follows that $h_{\mathbf{y}}(F)$ is a strictly concave function in F . Hence, we conclude that problem (18) is convex and has a unique solution.

Next, the proof that C in (18) is also given by $C = \sup_{F \in \mathcal{F}_A} I(F) - \sum_{l \in \{0\} \cup \mathcal{L}} \lambda_l g_l(F)$ follows from the Lagrangian theorem for constrained optimization problems. In particular, this equivalence holds for the convex

problem in (18) if C is finite and Slater's condition holds, i.e., if there exists an interior point $\tilde{F} \in \mathcal{F}_A$ such that all constraints hold with strict inequality, i.e., $g_l(\tilde{F}) < 0$, $\forall l \in \{0\} \cup \mathcal{L}$. The finiteness of the conditional capacity C is guaranteed by the AP constraint. Next, we prove that for the considered problem, Slater's condition holds. Let \tilde{x} satisfy $|\tilde{x}| < \sigma < A$ and $P_l(\tilde{x}) > P_{l,\text{req}}$, $\forall l \in \mathcal{L}$, and let \tilde{F} be the unit-step function at \tilde{x} , then $g_0(\tilde{F}) = \tilde{x}^2 - \sigma^2 < 0$ and $g_l(\tilde{F}) = -P_l(\tilde{x}) + P_{l,\text{req}} < 0$, $\forall l \in \mathcal{L}$, and hence, Slater's condition holds. Thus, from the Lagrangian theorem, strong duality holds, i.e., $\exists \lambda_l \geq 0$, $\forall l \in \{0\} \cup \mathcal{L}$, such that $C = \sup_{F \in \mathcal{F}_A} I(F) - \sum_{l \in \{0\} \cup \mathcal{L}} \lambda_l g_l(F)$ and is achieved also by F_0 . Moreover, the complementary slackness conditions $\lambda_l g_l(F_0) = 0$ must hold $\forall l \in \{0\} \cup \mathcal{L}$. This completes the proof.

APPENDIX B – PROOF OF THEOREM 2

Define $J(F) \triangleq I(F) - \sum_{l \in \{0\} \cup \mathcal{L}} \lambda_l g_l(F)$, then from Theorem 1, C can be written as $C = \sup_{F \in \mathcal{F}_A} J(F)$. From [25, Theorem 3], if \mathcal{F}_A is convex, and $J(F)$ is concave and weakly differentiable, then $J'_{F_0}(F) \leq 0$ is a necessary and sufficient condition for $J(F)$ to achieve its maximum at F_0 , where $J'_{F_0}(F) \triangleq \lim_{\theta \rightarrow 0} (J((1-\theta)F_0 + \theta F) - J(F_0))/\theta$ is the weak derivative of $J(F)$ at F_0 . In Appendix A, we established that \mathcal{F}_A is convex and that $J(F)$ is strictly concave in F , since $I(F)$ is strictly concave in F and $g_l(F)$ is affine in F $\forall l \in \{0\} \cup \mathcal{L}$. It remains to be proved that $J(F)$ is weakly differentiable and to determine the derivative $J'_{F_0}(F) = I'_{F_0}(F) - \sum_{l \in \{0\} \cup \mathcal{L}} \lambda_l g'_{l,F_0}(F)$. In [25, Proof of Theorem 3], it is shown that $I'_{F_0}(F)$ exists and is given by $I'_{F_0}(F) = \int i(x; F_0) dF(x) - I(F_0)$. It is also shown that for any linear constraint function $g_l(F)$, the derivative is $g'_{l,F_0}(F) = g_l(F) - g_l(F_0)$. From complementary slackness, $\lambda_l g_l(F_0) = 0$ $\forall l$. Hence, the condition $J'_{F_0}(F) \leq 0$ for the optimality of F_0 is $\int i(x; F_0) dF(x) - C - \sum_{l \in \{0\} \cup \mathcal{L}} \lambda_l g_l(F) \leq 0$, which reduces to (19). This completes the proof.

APPENDIX C – PROOF OF COROLLARY 1

We start with condition (19) which guarantees the optimality of F_0 . From Appendix B, (19) can be written as $\int i(x; F_0) dF(x) - C - \sum_{l \in \{0\} \cup \mathcal{L}} \lambda_l g_l(F) \leq 0$. Define $g_l(F) = \int A_l(x) dF(x) - a_l$, $l \in \{0\} \cup \mathcal{L}$. Hence, $A_0(x) = x^2$, $a_0 = \sigma^2$, $A_l(x) = -P_l(x)$, and $a_l = -P_{l,\text{req}}$, for $l \in \mathcal{L}$. Thus, (19) can be written as

$$\int \left(i(x; F_0) - \sum_{l \in \{0\} \cup \mathcal{L}} \lambda_l A_l(x) \right) dF(x) \leq C - \sum_{l \in \{0\} \cup \mathcal{L}} \lambda_l a_l. \quad (27)$$

Next, we prove that (27) holds if and only if

$$i(x; F_0) \leq C + \sum_{l \in \{0\} \cup \mathcal{L}} \lambda_l (A_l(x) - a_l), \quad \forall x \in [-A, A], \quad (28)$$

and

$$i(x; F_0) = C + \sum_{l \in \{0\} \cup \mathcal{L}} \lambda_l (A_l(x) - a_l), \quad \forall x \in E_0. \quad (29)$$

Clearly, if both conditions (28) and (29) hold, F_0 must be optimal because the necessary and sufficient condition in (27) is satisfied. The converse remains to be proved, i.e., if (27) holds, (28) and (29) must also hold. We prove this by contradiction. Assume that (27) holds but (28) does not. It means that $\exists \tilde{x} \in [-A, A]$ such that $i(\tilde{x}; F_0) > C + \sum_{l \in \{0\} \cup \mathcal{L}} \lambda_l (A_l(\tilde{x}) - a_l)$. Now, let F be the unit-step function at \tilde{x} , then the LHS of (27) becomes $i(\tilde{x}; F_0) - \sum_{l \in \{0\} \cup \mathcal{L}} \lambda_l A_l(\tilde{x}) > C - \sum_{l \in \mathcal{L}} \lambda_l a_l$, which violates (27). Hence, if (27) holds, (28) must also hold. Now, assume that (27) holds but (29) does not. That is, for a subset of E_0 defined as $E' \subset E_0$, with positive measure, i.e., $\int_{E'} dF_0(x) = \delta > 0$, (29) does not hold. Then, from (28), $i(x; F_0) < C + \sum_{l \in \{0\} \cup \mathcal{L}} \lambda_l (A_l(x) - a_l)$, $\forall x \in E'$. Since F_0 has points of increase on E_0 only, we have $\int_{E_0} dF_0(x) = \int_{E'} dF_0(x) + \int_{E_0 - E'} dF_0(x) = \delta + (1 - \delta) = 1$. Now, we can write $C - \sum_{l \in \{0\} \cup \mathcal{L}} \lambda_l a_l \leq I(F_0) - \sum_{l \in \{0\} \cup \mathcal{L}} \lambda_l \int A_l(x) dF_0(x) = \int (i(x; F_0) - \sum_{l \in \{0\} \cup \mathcal{L}} \lambda_l A_l(x)) dF_0(x)$, as

$$\begin{aligned} C - \sum_{l \in \{0\} \cup \mathcal{L}} \lambda_l a_l &\leq \underbrace{\int_{x \in E'} (i(x; F_0) - \sum_{l \in \{0\} \cup \mathcal{L}} \lambda_l A_l(x)) dF_0(x)}_{< \delta(C - \sum_{l \in \{0\} \cup \mathcal{L}} \lambda_l a_l)} \\ &+ \underbrace{\int_{x \in E_0 - E'} (i(x; F_0) - \sum_{l \in \{0\} \cup \mathcal{L}} \lambda_l A_l(x)) dF_0(x)}_{=(1-\delta)(C - \sum_{l \in \{0\} \cup \mathcal{L}} \lambda_l a_l)} < C - \sum_{l \in \{0\} \cup \mathcal{L}} \lambda_l a_l, \end{aligned}$$

which is a contradiction. Hence, if (27) holds, (29) must also hold. Therefore, (28) and (29) are necessary and sufficient conditions for the optimality of the input distribution F_0 . Next, we obtain condition (20) from (28) and (29). By definition, the marginal information density $i(x, F_0)$ is given by [22]

$$\begin{aligned} i(x, F_0) &= \int_y p(y|x) \log_2 \left(\frac{p(y|x)}{p(y; F_0)} \right) dy \\ &= \int p(y|x) \log_2(p(y|x)) dy - \int p(y|x) \log_2(p(y; F_0)) dy \\ &= -\frac{1}{2} \log_2(2\pi e \sigma_n^2) - \int \frac{e^{-\frac{(y-xh_1)^2}{2\sigma_n^2}}}{\sqrt{2\pi\sigma_n^2}} \log_2(p(y; F_0)) dy, \end{aligned} \quad (30)$$

where the first term on the RHS is the negative of the entropy of the noise. Finally, using the definitions of $A_l(x)$ and a_l for $l \in \{0\} \cup \mathcal{L}$, (28) and (29) reduce to (20). This completes the proof.

APPENDIX D – PROOF OF THEOREM 3

Our proof of the discreteness and finiteness of the optimal input distribution parallels that in [25] and [26, Section IV]. Specifically, we prove by contradiction that the set of mass points E_0 of the optimal input distribution must be discrete with finite number of mass points. In particular, assuming E_0 is continuous or discrete with infinite number of mass points, then according to the Bolzano-Weierstrass theorem, since $E_0 \subset [-A, A]$, i.e., E_0 is bounded, E_0 must have an accumulation point

[22]. On the other hand, from Corollary 1, a necessary condition for the optimal input distribution to be F_0 is that $s(x)$ in (20) must be zero, $\forall x \in E_0$. Hence, $s(x)$ must be zero on an infinite set of points having an accumulation point. Next, we extend $s(x)$ in (20) to the complex domain, i.e.,

$$\begin{aligned} s(z) &\triangleq \lambda_0(z^2 - \sigma^2) - \sum_{l \in \mathcal{L}} \lambda_l (P_l(z) - P_{l, \text{req}}) + C \\ &+ \frac{1}{2} \log_2(2\pi e \sigma_n^2) + \frac{1}{\sqrt{2\pi\sigma_n^2}} \int e^{-\frac{(y-zh_1)^2}{2\sigma_n^2}} \log_2(p(y; F_0)) dy, \end{aligned} \quad (31)$$

where $z \in \mathbb{C}$. The extension to the complex domain is necessary to use the identity theorem for analytic functions in complex analysis. In particular, we first establish the analyticity of function $s(z)$. In (31), the quadratic function, the exponential function, and their compositions are analytic functions in the whole complex domain $z \in \mathbb{C}$ [22]. In $P_l(z) = \min \left(\left[\frac{1}{a} W_0(ae^a I_0(\sqrt{2} B h_{E_l} z)) - 1 \right]^2 i_s^2 R_L, \frac{B^2}{4R_L} \right)$, defined in (15), the $\min(\cdot)$ function, the quadratic function $(\cdot)^2$, the modified Bessel function $I_0(\cdot)$, and their compositions are analytic on the whole complex domain $z \in \mathbb{C}$. The principal branch of the LambertW function $W_0(\cdot)$ is analytic everywhere in the complex domain with the exception of the branch cut along the negative real axis, i.e., on $(-\infty, -1/e)$ [29], [35]. Hence, the function $s(z)$ is analytic in the domain D defined by $D \triangleq \{z \in \mathbb{C} : ae^a I_0(\sqrt{2} B h_{E_l} z) \in \mathbb{C} \setminus (-\infty, -1/e), \forall l \in \mathcal{L}\}$. Thus, we have an analytic function $s(z)$ in a domain D that is zero over an infinite set of points E_0 having an accumulation point in D . By the identity theorem [23], [25], function $s(z)$ must be zero in the whole domain D , i.e., $s(z) = 0$, $\forall z \in D$. Next, we show that this condition is invalid over a subset of D , which violates the original assumption on E_0 being continuous or discrete with infinite number of mass points.

First, we restrict our attention to $z \in \mathbb{R}$ which is a subset¹⁴ of D and solve for the unknown distribution $p(y; F_0)$ in (31) for which $s(z) = 0$. Similar to [26], we set $\sigma_n^2 = 1$ to simplify the proof without loss of generality (w.l.o.g.) and express the last integral term in (31) in terms of the Hermite polynomials $H_m(y)$ defined in [26, Appendix F]. In particular, since $\log_2(p(y; F_0))$ is a continuous function of y and is square integrable with respect to $e^{-y^2/2}$, it can be written as $\log_2(p(y; F_0)) = \sum_{m=0}^{\infty} c_m H_m(y)$, where c_m are constants. Hence, the last term of $s(z)$ in (31) can be written as $Z \triangleq \frac{1}{\sqrt{2\pi}} \int e^{-\frac{y^2}{2}} e^{-\frac{(h_1 z)^2}{2}} + h_1 z y \log_2(p(y; F_0)) dy = \frac{1}{\sqrt{2\pi}} \int e^{-\frac{y^2}{2}} \sum_{n=0}^{\infty} \frac{(h_1 z)^n}{n!} H_n(y) \sum_{m=0}^{\infty} c_m H_m(y) dy$, where we used the Hermite polynomial expansion $e^{-(h_1 z)^2/2} + h_1 z y = \sum_{n=0}^{\infty} \frac{(h_1 z)^n}{n!} H_n(y)$ [26].

Using the orthogonality of the Hermite polynomials with $e^{-y^2/2}$ given by $\int_{-\infty}^{\infty} H_n(y) H_m(y) e^{-y^2/2} dy = m! \sqrt{2\pi}$ if $m = n$ and zero otherwise [26, Appendix

¹⁴ $\mathbb{R} \subset D$ since for $z \in \mathbb{R}$, the argument of $W_0(\cdot)$ is $ae^a I_0(\sqrt{2} B h_{E_l} z) \in (ae^a, \infty) \subset \mathbb{R}^+$, i.e., it is in the analytical domain of $W_0(\cdot)$.

F], then Z reduces to $Z = \sum_{m=0}^{\infty} c_m (h_l z)^m$. Next, we replace $P_l(z)$ by its Taylor series to write $s(z)$ in (31) in a polynomial form. In particular, the LambertW function admits a convergent Taylor series around an arbitrary point $x_0 \in \mathbb{R}$ given by [35, Eq. (8), (10)]

$$W_0(x) = \sum_{n=1}^{\infty} \frac{e^{-nW_0(x_0)}}{(1+W_0(x_0))^{2n-1}} \frac{p_n(W_0(x_0))}{n!} (x-x_0)^n \\ + W_0(x_0) \triangleq \sum_{n=0}^{\infty} d_n(x_0)x^n, \quad |x-x_0| < x_{\text{ROC}},$$

where $p_n(\cdot)$ is a polynomial with coefficients given in [35, Table I.]. This series holds for some radius of convergence (ROC) $|x-x_0| < x_{\text{ROC}}$ and can be expanded to a polynomial in x defined as $W_0(x) = \sum_{n=0}^{\infty} d_n(x_0)x^n$. Moreover, using the Taylor series expansion of the modified Bessel function given by $I_0(z) = \sum_{m=0}^{\infty} \frac{(z/2)^{2m}}{(m!)^2}$, the Bessel function in $P_l(z)$ can be written as $I_0(\sqrt{2}Bh_{E_l}z) = \sum_{m=0}^{\infty} \alpha_{m,l}z^{2m}$, where $\alpha_{m,l} = \frac{(Bh_{E_l}/\sqrt{2})^{2m}}{(m!)^2}$. Hence, the harvested power function $P_l(z)$ in (15) is a quadratic function of a polynomial of another polynomial function with even powers of z . Thus, $P_l(z)$ can be written as

$$P_l(z) = \min \left(\left[\frac{1}{a} \sum_{n=0}^{\infty} d_n(x_0) \left(ae^a \sum_{m=0}^{\infty} \alpha_{m,l} z^{2m} \right)^n - 1 \right]^2 i_s^2 R_L, \frac{B_v^2}{4R_L} \right) \triangleq \min \left(\sum_{m=0}^{\infty} q_{m,l} z^{2m}, \frac{B_v^2}{4R_L} \right), \quad (32)$$

where $q_{m,l} \in \mathbb{R}$ and (32) holds for $|ae^a I_0(\sqrt{2}Bh_{E_l}z) - x_0| < x_{\text{ROC}}$. From (31), $s(z)=0$ reduces to

$$\sum_{m=0}^{\infty} c_m h_l^m z^m = \sum_{l \in \mathcal{L}} \lambda_l \left(\min \left(\sum_{m=0}^{\infty} q_{m,l} z^{2m}, \frac{B_v^2}{4R_L} \right) - P_{l,\text{req}} \right) \\ - \lambda_0 (z^2 - \sigma^2) - C - \frac{1}{2} \log_2(2\pi e). \quad (33)$$

Equating the coefficients of z^m , we get $c_m = 0$ for odd m . To obtain c_m for even m , let $A \geq A_{\text{T,sat}_l}$, $\forall l \in \mathcal{L}_{\text{sat}}$, i.e., with $P_l(z) = \frac{B_v^2}{4R_L}$, and $A < A_{\text{T,sat}_l}$, $\forall l \in \mathcal{L}_{\text{non-sat}}$, then

$$c_0 = \left(\sum_{l \in \mathcal{L}_{\text{non-sat}}} \lambda_l q_{0,l} + \sum_{l \in \mathcal{L}_{\text{sat}}} \lambda_l \frac{B_v^2}{4R_L} - \sum_{l \in \mathcal{L}} \lambda_l P_{l,\text{req}} \right) \\ + \lambda_0 \sigma^2 - C - 0.5 \log_2(2\pi e), \\ c_2 = \left(\sum_{l \in \mathcal{L}_{\text{non-sat}}} \lambda_l q_{2,l} - \lambda_0 \right) / h_1^2, \\ c_m = \sum_{l \in \mathcal{L}_{\text{non-sat}}} \frac{\lambda_l q_{\frac{m}{2},l}}{h_1^m}, \quad \forall m \geq 4. \quad (34)$$

Using (34), the output pdf in $\log_2(p(y; F_0)) = \sum_{m=0}^{\infty} c_m H_m(y)$ reduces to $p(y; F_0) = e^{\ln(2) \sum_{n=0}^{\infty} c_{2n} H_{2n}(y)}$. Next, we consider two cases based on whether or not the EH constraints are active.

We will show that in both cases, the optimal input distribution is discrete with finite number of mass points. *Case 1* ($\lambda_l = 0$, $\forall l \in \mathcal{L}$): If all EH constraints are inactive, i.e., they are satisfied with strict inequality, then $\lambda_l = 0$, $\forall l \in \mathcal{L}$, from the complementary slackness, cf. Theorem 1. In this case, the coefficients in (34) reduce to $c_0 = \lambda_0 \sigma^2 - C - 0.5 \log_2(2\pi e)$, $c_2 = -\lambda_0/h_1^2$, and $c_m = 0$, $\forall m \neq \{0, 2\}$. Using the Hermite polynomials $H_0(y) = 1$, $H_2(y) = y^2 - 1$ [26, Appendix F], the output pdf reduces to $p(y; F_0) = e^{\ln(2)(c_0 - c_2)} e^{\ln(2)c_2 y^2}$. Since the support of $p(y; F_0)$ is the whole real line \mathbb{R} and $c_2 < 0$, this output distribution is the Gaussian distribution with zero mean. Now, for \mathbf{y} to be Gaussian distributed for the AWGN channel model $\mathbf{y} = \mathbf{x}h_1 + \mathbf{n}$, \mathbf{x} must also be Gaussian distributed. However, with the PP constraint $|\mathbf{x}| \leq A$, \mathbf{x} cannot be Gaussian distributed on a bounded interval. Thus, the obtained output distribution is invalid. Hence, the condition $s(z) = 0$ is invalid on a subset of the domain D defined by the region of convergence of (32). This contradicts the original assumption that E_0 is continuous or discrete with infinite number of mass points. Therefore, E_0 must be discrete with finite number of mass points.

Case 2 ($\lambda_l > 0$, $l \in \mathcal{L}_A \subset \mathcal{L}$): In this case, some of the EH constraints are active, i.e., $\forall l \in \mathcal{L}_A$, C_l in (18) is satisfied with equality and the coefficients c_m are given by (34). From [26], the Hermite polynomials of even orders are function of even powers of y . Thus, the output distribution reduces to $p(y; F_0) = e^{\ln(2) \sum_{n=0}^{\infty} t_n y^{2n}} = \prod_{n=0}^{\infty} e^{\ln(2)t_n y^{2n}}$, where t_n are non-zero constants. It can be verified that for some $n \rightarrow \infty$, $\exists t_n > 0$, in which case $p(y; F_0)$ cannot be a valid distribution since it is unbounded. Hence, we conclude that the set E_0 must be discrete and finite. This completes the proof.

APPENDIX E – PROOF OF THEOREM 4

Consider problem (18) with $A < A_{\text{sat}}$. Assume that only one EH Rx, having index 1, requires a certain average harvested power $P_{1,\text{req}}$ and the remaining EH Rxs passively harvest energy from their received signals. Assume further that EH constraint C_1 is feasible and active and the optimal distribution is F_1 . The average harvested powers at the EH Rxs are $\mathbb{E}_{F_1}[P_l(\mathbf{x})]$, $\forall l \in \mathcal{L}$. Next, we show that if another feasible EH constraint C_2 is added to problem (18), then at most one of the two constraints, denoted by C_a , is active. In particular, we add constraint C_2 for EH Rx 2 with required average harvested power $P_{2,\text{req}}$. In this case, if $P_{2,\text{req}} < \mathbb{E}_{F_1}[P_2(\mathbf{x})]$, then F_1 remains the optimal distribution and the EH constraint C_2 is inactive, i.e., $C_a = C_1$. Otherwise, if $P_{2,\text{req}} > \mathbb{E}_{F_1}[P_2(\mathbf{x})]$, then distribution F_1 fails to satisfy the EH requirement of EH Rx 2 and a more energy-biased distribution is needed. In this case, if problem (18) with only the EH constraint for EH Rx 2 is feasible with optimal distribution F_2 , then F_2 is more energy-biased but also less information-biased compared to F_1 . In particular, according to Lemma 1, $P_{2,\text{req}} = \mathbb{E}_{F_2}[P_2(\mathbf{x})] > \mathbb{E}_{F_1}[P_2(\mathbf{x})]$ also implies

$\mathbb{E}_{F_2}[P_1(x)] > \mathbb{E}_{F_1}[P_1(x)] = P_{1,\text{req}}$, i.e., using F_2 , the EH constraint of EH Rx 1 is satisfied with strict inequality. Hence, C_1 is inactive and only C_2 is active, i.e., $C_a = C_2$. The same discussion holds for constraint C_a and any other added constraint C_3 . Hence, by induction, at most one of the EH constraints in problem (18) is active. Moreover, due to the R-E tradeoff, a more energy-biased input distribution implies a lower information rate at the ID Rx, e.g., if $\mathbb{E}_{F_2}[P_l(x)] > \mathbb{E}_{F_1}[P_l(x)]$, then $I(F_2) < I(F_1)$ holds. Hence, the active EH constraint is the one, which when all other EH constraints are removed, leads to the lowest achievable rate at the ID Rx. This completes the proof.

APPENDIX F – PROOF OF THEOREM 5

Consider first the case when $A < A_{T,\text{sat}_l}$. Suppose x_0 is a point of increase of distribution F_0 having probability p_0 , where $0 < x_0 < A$. Thereby, we introduce a new distribution F_A which is constructed from F_0 by removing the mass point at x_0 and increasing the probabilities of mass points 0 and A by $p_0 - p_0 x_0^2/A^2$ and $p_0 x_0^2/A^2$, respectively. This transformation maintains the unity of the sum of probabilities of the mass points and ensures that the AP and PP constraints hold. Next, we show that if $P_l(0) = 0$ and $P_l(x)/x^2$ is a monotonically increasing function in $0 < x < A$, then the contribution of the mass points at $x = 0$ and $x = A$ to the average harvested power is higher than the contribution of any other point $x_0 \in (0, A)$. In particular,

$$\begin{aligned} p_0 P_l(x_0) &< p_0 \frac{x_0^2}{A^2} P_l(A) + p_0 \left(1 - \frac{x_0^2}{A^2}\right) P_l(0) \\ \Rightarrow \frac{P_l(x_0)}{x_0^2} &< \frac{P_l(A)}{A^2}, \end{aligned} \quad (35)$$

Condition (35) holds for the harvested power function in (15) since (a) $P_l(0) = 0$, as $I_0(0) = 1$ and $W_0(ae^a) = a$ and (b) $P_l(x)/x^2$ increases monotonically in $0 < x < A$. We derive this monotonicity by proving that $xP'_l(x) - 2P_l(x) > 0$ holds for $0 < x < A$, where $P'_l(x)$ is the first-order derivative of $P_l(x)$. In particular, this condition can be expressed as $D(x) \triangleq \left[\frac{u_l x I_1(u_l x)}{I_0(u_l x)[1 + W_0(ae^a I_0(u_l x))]} - 1 \right] \frac{W_0(ae^a I_0(u_l x))}{a} > -1$, $\forall x$, $0 < x < A$, where $u_l \triangleq \sqrt{2} B h_{E_l}$. It can be shown that $D(x)$ equals -1 for $x = 0$ and is larger than -1 for $x > 0$. Moreover, since the harvested power is an even function of x , i.e., $P_l(x) = P_l(-x)$, the weight of the mass point at A can be arbitrarily distributed between A and $-A$. To satisfy the AP constraint in (21) with equality, the total weights on the peak amplitudes A and $-A$ should satisfy $p + q = \min\{\sigma^2/A^2, 1\}$. Consider next the case when $A \geq A_{T,\text{sat}_l}$. For $x_0 \in (0, A_{T,\text{sat}_l})$, since $P_l(x)/x^2$ increases monotonically in $0 \leq x < A_{T,\text{sat}_l}$, similar to (35), the contribution of the mass points at $x = 0$ and $x = A_{T,\text{sat}_l}$ to the average harvested power is higher than the contribution of any other point $x_0 \in (0, A_{T,\text{sat}_l})$, since $\frac{P_l(x_0)}{x_0^2} < \frac{P_l(A_{T,\text{sat}_l})}{A_{T,\text{sat}_l}^2}$. On the other hand, for $x_0 \in (A_{T,\text{sat}_l}, A)$, $P_l(x_0)$ is constant, i.e., $P_l(x_0) = P_l(A_{T,\text{sat}_l}) = B_v^2/(4R_L)$. In

this case, $\frac{P_l(x_0)}{x_0^2} < \frac{P_l(A_{T,\text{sat}_l})}{A_{T,\text{sat}_l}^2}$ since $\frac{1}{x_0^2} < \frac{1}{A_{T,\text{sat}_l}^2}$, i.e., $P_l(x)/x^2 \propto 1/x^2$ is monotonically decreasing in x , for $x \geq A_{T,\text{sat}_l}$. As a result the contribution of the mass points at $x = 0$ and $x = A_{T,\text{sat}_l}$ to the average harvested power is higher than the contribution of any other point $x_0 \in (A_{T,\text{sat}_l}, A)$. This leads to the EH maximizing distribution given in (22). This completes the proof.

APPENDIX G – PROOF OF LEMMA 2

The proof of the optimality of input signals with independent amplitude and phase distributions parallels that in [23, Section II.B]. We start by expressing the mutual information as [23, eq. (6)]

$$\begin{aligned} I(\mathbf{y}; \mathbf{x}) &= H(\mathbf{y}) - H(\mathbf{n}) \\ &= H(\mathbf{R}, \boldsymbol{\psi}) + \int_{R=0}^{\infty} f_{\mathbf{R}}(R) \log_2(R) dR - \log_2(2\pi e \sigma_n^2). \end{aligned} \quad (36)$$

We note that the joint entropy $H(\mathbf{R}, \boldsymbol{\psi})$ is maximized for independent \mathbf{R} and $\boldsymbol{\psi}$ with a maximum of $\max(H(\mathbf{R}, \boldsymbol{\psi})) = H(\mathbf{R}) + H(\boldsymbol{\psi})$, and the entropy $H(\boldsymbol{\psi})$ is maximized for a uniformly distributed phase $\boldsymbol{\psi}$ with a maximum of $\max(H(\boldsymbol{\psi})) = \log_2(2\pi)$. Hence, we have

$$\begin{aligned} \sup H(\mathbf{R}, \boldsymbol{\psi}) &= \sup H(\mathbf{R}) + \log_2(2\pi) \\ &= \sup \left\{ - \int_{R=0}^{\infty} f_{\mathbf{R}}(R) \log_2(f_{\mathbf{R}}(R)) dR \right\} + \log_2(2\pi), \end{aligned} \quad (37)$$

which when combined with (36) results in

$$\begin{aligned} \sup I(\mathbf{y}; \mathbf{x}) &= \sup I(F_{\mathbf{r}}) \\ &= \sup \left\{ - \int_{R=0}^{\infty} f_{\mathbf{R}}(R; F_{\mathbf{r}}) \log_2 \left(\frac{f_{\mathbf{R}}(R; F_{\mathbf{r}})}{R} \right) dR \right\} - \log_2(e \sigma_n^2), \end{aligned} \quad (38)$$

where $F_{\mathbf{r}}$ in $f_{\mathbf{R}}(R; F_{\mathbf{r}})$ is used to emphasize that $f_{\mathbf{R}}(R)$ depends on $F_{\mathbf{r}}$. Similar to [23, eq. (11)],

$$f_{\mathbf{R}|\mathbf{r}, \boldsymbol{\theta}}(R, \boldsymbol{\psi}|r, \theta) = \frac{R}{2\pi \sigma_n^2} e^{-\frac{(R^2 + r^2 |h_1|^2 - 2Rr|h_1| \cos(\psi - \theta - \phi))}{2\sigma_n^2}}. \quad (39)$$

Furthermore, similar to [23, eq. (10)], it can be shown that

$$\begin{aligned} f_{\mathbf{R}}(R; F_{\mathbf{r}}) &= \int_{r=0}^A \frac{R}{\sigma_n^2} e^{-\frac{R^2 + r^2 |h_1|^2}{2\sigma_n^2}} I_0 \left(\frac{Rr|h_1|}{\sigma_n^2} \right) dF_{\mathbf{r}}(r) \\ &\triangleq \int_{r=0}^A K(r, R) dF_{\mathbf{r}}(r). \end{aligned} \quad (40)$$

Hence, it is concluded that $f_{\mathbf{R}}(R; F_{\mathbf{r}})$ is independent of $F_{\boldsymbol{\theta}}(\boldsymbol{\theta})$. Next, we prove that selecting independent \mathbf{r} and $\boldsymbol{\theta}$, with uniformly distributed $\boldsymbol{\theta}$, i.e., $d^2 F_{\mathbf{r}, \boldsymbol{\theta}}(r, \theta) = \frac{1}{2\pi} d\theta dF_{\mathbf{r}}(r)$, results in independent \mathbf{R} and $\boldsymbol{\psi}$, with uniformly distributed $\boldsymbol{\psi}$, i.e., $f_{\mathbf{R}, \boldsymbol{\psi}}(R, \boldsymbol{\psi}) = \frac{1}{2\pi} f_{\mathbf{R}}(R; F_{\mathbf{r}})$.

In particular, using (39) and (40), we get

$$\begin{aligned} f_{\mathbf{R},\psi}(R, \psi) &= \int_{r=0}^A \int_{\theta=-\pi}^{\pi} f_{\mathbf{R},\psi|\mathbf{r},\theta}(R, \psi|r, \theta) d^2F_{\mathbf{r},\theta}(r, \theta) \\ &= \int_{r=0}^A \frac{R}{2\pi\sigma_n^2} e^{-\frac{R^2+r^2|h_1|^2}{2\sigma_n^2}} I_0\left(\frac{Rr|h_1|}{\sigma_n^2}\right) dF_{\mathbf{r}}(r) = \frac{1}{2\pi} f_{\mathbf{R}}(R; F_{\mathbf{r}}), \end{aligned} \quad (41)$$

which, from (37) and (38), maximizes the joint entropy $H(\mathbf{R}, \psi)$ and the mutual information $I(F_{\mathbf{r}})$. Hence, independent \mathbf{r} and θ with uniformly distributed θ are optimal. This completes the proof.

APPENDIX H – PROOF OF THEOREM 6

The proof of the uniqueness of the solution of problem (25) is similar to that in Appendix A. In particular, the constraints in (25) are convex and compact in $F_{\mathbf{r}}$. From (38), $I(F_{\mathbf{r}})$ can be written as

$$\begin{aligned} I(F_{\mathbf{r}}) &= -\int_{\nu=0}^{\infty} f_{\nu}(\nu; F_{\mathbf{r}}) \log_2(f_{\nu}(\nu; F_{\mathbf{r}})) d\nu - \log_2(e\sigma_n^2) \\ &\triangleq h(\nu; F_{\mathbf{r}}) - \log_2(e\sigma_n^2), \end{aligned} \quad (42)$$

where we used the change of variables $\nu = R^2/2$, hence $f_{\mathbf{R}}(R; F_{\mathbf{r}})/R = f_{\nu}(\nu; F_{\mathbf{r}})$ and $d\nu = R dR$. Hence, the mutual information depends on the entropy associated with random variable ν which is strictly concave in $F_{\mathbf{r}}$. Therefore, the solution to problem (25) is unique. From (38) and (40), $I(F_{\mathbf{r}})$ can be written as

$$\begin{aligned} I(F_{\mathbf{r}}) &= -\int_{R=0}^A \int_{r=0}^A K(r, R) \log_2\left(\frac{f_{\mathbf{R}}(R; F_{\mathbf{r}})}{R}\right) dR dF_{\mathbf{r}}(r) - \log_2(e\sigma_n^2) \\ &= \int_{r=0}^A \left(-\int_{R=0}^A K(r, R) \log_2\left(\frac{f_{\mathbf{R}}(R; F_{\mathbf{r}})}{R}\right) dR - \log_2(e\sigma_n^2) \right) dF_{\mathbf{r}}(r) \\ &\triangleq \int_{r=0}^A i(r; F_{\mathbf{r}}) dF_{\mathbf{r}}(r), \end{aligned} \quad (43)$$

where we used $\int_{r=0}^A dF_{\mathbf{r}}(r) = 1$. Next, we obtain the necessary and sufficient conditions for the input distribution $F_{\mathbf{r}_0}(r)$ to be optimal. These conditions correspond to those in Theorem 2 and Corollary 1 but for the input amplitude r . In particular, with the definition of $I(F_{\mathbf{r}})$ in (43), the complex signaling problem in (25) is symbolically equivalent to that with real signaling in (18) after replacing random variable $\mathbf{x} \in [-A, A]$ by $\mathbf{r} \in [0, A]$ and using the marginal mutual information $i(r; F_{\mathbf{r}})$ in (43). Following Appendices B and C, the conditions in (28) and (29) generalize to $i(r; F_{\mathbf{r}_0}) \leq C + \sum_{l \in \{0\} \cup \mathcal{L}} \lambda_l (A_l(r) - a_l)$, $\forall r \in [0, A]$, where equality holds if $r \in E_0$. Substituting with $A_0(r) = r^2$, $a_0 = \sigma^2$, $A_l(r) = -P_l(r)$, $a_l = -P_{l,\text{req}}$, $l \in \mathcal{L}$, $i(r; F_{\mathbf{r}_0})$ from (43), and $K(r, R)$ from (40), we obtain (26).

Next, we prove that the optimal input distribution must be discrete with finite number of mass points. Similar to Appendix D, we prove that the complex extension of $s(r)$ in (26) cannot be zero over an infinite set of points having an accumulation point and hence E_0 must be discrete

and finite. For simplicity and w.l.o.g., we set $\sigma_n^2 = 1$. Extending $s(r)$ in (26) to the complex z domain, we can write $s(z) = 0$ as

$$\begin{aligned} &\int_0^{\infty} Q(\nu, z|h_1|) \log_2(f_{\nu}(\nu; F_{\mathbf{r}_0})) d\nu \\ &= -\lambda_0(z^2 - \sigma^2) + \sum_{l \in \mathcal{L}} \lambda_l(P_l(z) - P_{l,\text{req}}) - C - \log_2(e), \end{aligned} \quad (44)$$

where we used $\nu = R^2/2$, hence $f_{\mathbf{R}}(R; F_{\mathbf{r}})/R = f_{\nu}(\nu; F_{\mathbf{r}})$ and $d\nu = R dR$ and we define the kernel $Q(\nu, z|h_1|)$ as $Q(\nu, z|h_1|) \triangleq e^{-\nu - \frac{z^2|h_1|^2}{2}} I_0(\sqrt{2\nu}z|h_1|)$. The analyticity of the RHS of (44) is proved in Appendix D. The LHS of (44) is analytic in $z \in \mathbb{C}$, which follows by the differentiation lemma and the Schwarz property of the kernel $Q(\nu, z|h_1|)$ [23, Appendix I]. Hence, $s(z)$ is analytic over domain D defined in Appendix D. Thus, from the identity theorem [23], [25], if $s(z) = 0 \forall z \in E_0$ and E_0 is an infinite set of points with an accumulation point, then $s(z) = 0, \forall z \in D$. Next, we restrict our attention to $z \in \mathbb{R} \subset D$ and check if there exists a valid output pdf $f_{\nu}(\nu; F_{\mathbf{r}_0})$ that satisfies (44). Eq. (44) is an integral transform which was proved in [23, Appendix II] to be invertible, i.e., there exists a unique solution for the unknown function $f_{\nu}(\nu; F_{\mathbf{r}_0})$ ¹⁵. Applying the integral transform to the power function ν^n , we get $\int_0^{\infty} Q(\nu, z|h_1|) \nu^n d\nu = n! L_n(-z^2|h_1|^2/2)$, where $L_n(\cdot)$ is the Laguerre Polynomial defined as $L_n(x) = \sum_{m=0}^n \binom{n}{m} \frac{(-1)^m}{m!} x^m$. Hence, the integral transform of the polynomial $\sum_{n=0}^{\infty} c_n \nu^n$ is

$$\int_0^{\infty} Q(\nu, z|h_1|) \sum_{n=0}^{\infty} c_n \nu^n d\nu = \sum_{n=0}^{\infty} c_n n! L_n(-z^2|h_1|^2/2). \quad (45)$$

If there exist coefficients c_n such that the RHS of (44) equals the RHS of (45), then the unique solution of $f_{\nu}(\nu; F_{\mathbf{r}_0})$ must satisfy $\log_2(f_{\nu}(\nu; F_{\mathbf{r}_0})) = \sum_{n=0}^{\infty} c_n \nu^n$. Next, we write the RHS of (44) in a polynomial form, and check whether this polynomial can be written as a weighted sum of Laguerre polynomials as in the RHS of (45). Using $P_l(z) = \min(\sum_{m=0}^{\infty} q_{m,l} z^{2m}, B_v^2/(4R_L))$ from (32), we write the RHS of (44) as $\sum_{m=0}^{\infty} \alpha_m z^{2m}$, where $\alpha_0 = \lambda_0 \sigma^2 + \left(\sum_{l \in \mathcal{L}_{\text{non-sat}}} \lambda_l q_{0,l} + \sum_{l \in \mathcal{L}_{\text{sat}}} \lambda_l B_v^2/(4R_L) - \sum_{l \in \mathcal{L}} \lambda_l P_{l,\text{req}} \right) - C - \log_2(e)$, $\alpha_1 = -\lambda_0 + \sum_{l \in \mathcal{L}_{\text{non-sat}}} \lambda_l q_{1,l}$, and $\alpha_m = \sum_{l \in \mathcal{L}_{\text{non-sat}}} \lambda_l q_{m,l} \forall m \geq 2$. Hence, (44) can be written as

$$\int_0^{\infty} Q(\nu, z|h_1|) \log_2(f_{\nu}(\nu; F_{\mathbf{r}_0})) d\nu = \sum_{m=0}^{\infty} \alpha_m z^{2m}. \quad (46)$$

Hence, the problem reduces to finding the coefficients c_n that make the RHSs of (45) and (46) equal. Using

¹⁵Unlike with real signaling, where $f_{\nu}(\nu; F_{\mathbf{r}_0})$ was obtained in terms of the Hermite polynomials, with complex signaling, the kernel $Q(\nu, z|h_1|)$ is not orthogonal to the Hermite polynomials. Hence, we use a different approach to obtain $f_{\nu}(\nu; F_{\mathbf{r}_0})$.

the definition of the Laguerre polynomial, we require $\sum_{m=0}^{\infty} \alpha_m z^{2m} = \sum_{n=0}^{\infty} c_n n! \sum_{m=0}^n \binom{n}{m} \frac{|h_1|^{2m}}{m! 2^m} z^{2m}$. Thus, c_n satisfies the linear system of equations $\alpha_m = \sum_{n=m}^{\infty} c_n n! \binom{n}{m} \frac{|h_1|^{2m}}{m! 2^m}$, $m = 0, \dots, \infty$. Truncating the summation order to $2S$ for some large S , the linear system of equations can be written as $\alpha = M\mathbf{c}$, where $\alpha = [\alpha_0, \dots, \alpha_S]^T$, $\mathbf{c} = [c_0, \dots, c_S]^T$, and M is an upper triangular matrix whose non-zero entries in the m^{th} row and the n^{th} column are $n! \binom{n}{m} \frac{|h_1|^{2m}}{m! 2^m}$, for $n \geq m$ and zero, otherwise. Since any upper triangular matrix with non-zero main diagonal entries is invertible, the coefficients c_n can be obtained uniquely as $\mathbf{c} = M^{-1}\alpha$. Using these coefficients, the RHSs of (45) and (46) are equal, and therefore their LHSs are also equal, i.e., $f_{\nu}(\nu; F_{\mathbf{r}_0}) = e^{\ln(2) \sum_{n=0}^{\infty} c_n \nu^n}$, which does not correspond to a legitimate pdf. Hence, (44) cannot hold over an infinite set of points with an accumulation point, i.e., E_0 must be discrete and finite. This completes the proof.

REFERENCES

- [1] R. Morsi, V. Jamali, D. W. K. Ng, and R. Schober, "On the Capacity of SWIPT Systems with a Nonlinear Energy Harvesting Circuit," in *Proc. IEEE Intern. Commun. Conf.*, May 2018, pp. 1–7.
- [2] L. R. Varshney, "Transporting Information and Energy Simultaneously," in *Proc. IEEE Intern. Sympos. on Inf. Theory*, Jul. 2008, pp. 1612–1616.
- [3] P. Grover and A. Sahai, "Shannon Meets Tesla: Wireless Information and Power Transfer," in *Proc. IEEE Intern. Sympos. on Inf. Theory*, Jun. 2010, pp. 2363–2367.
- [4] R. Zhang and C. K. Ho, "MIMO Broadcasting for Simultaneous Wireless Information and Power Transfer," *IEEE Trans. Wireless Commun.*, vol. 12, no. 5, pp. 1989–2001, May 2013.
- [5] Z. Ding, C. Zhong, D. W. K. Ng, M. Peng, H. A. Suraweera, R. Schober, and H. V. Poor, "Application of Smart Antenna Technologies in Simultaneous Wireless Information and Power Transfer," *IEEE Commun. Mag.*, vol. 53, no. 4, pp. 86–93, Apr. 2015.
- [6] D. Ng, T. Duong, C. Zhong, and R. Schober, *Wireless Information and Power Transfer: Theory and Practice*, ser. Wiley - IEEE. Wiley, 2019.
- [7] Z. Wei, X. Zhu, S. Sun, Y. Jiang, A. Al-Tahmeesschi, and M. Yue, "Research Issues, Challenges, and Opportunities of Wireless Power Transfer-Aided Full-Duplex Relay Systems," *IEEE Access*, vol. 6, pp. 8870–8881, 2018.
- [8] J. Kang, I. Kim, and D. I. Kim, "Wireless Information and Power Transfer: Rate-Energy Tradeoff for Nonlinear Energy Harvesting," *IEEE Trans. Wireless Commun.*, vol. 17, no. 3, pp. 1966–1981, Mar. 2018.
- [9] B. Clerckx, "Wireless Information and Power Transfer: Nonlinearity, Waveform Design, and Rate-Energy Tradeoff," *IEEE Trans. Signal Process.*, vol. 66, no. 4, pp. 847–862, Feb. 2018.
- [10] M. Varasteh, B. Rassouli, and B. Clerckx, "Wireless Information and Power Transfer over an AWGN Channel: Nonlinearity and Asymmetric Gaussian Signaling," in *Proc. IEEE Inf. Theory Workshop*, Nov. 2017, pp. 181–185.
- [11] B. Clerckx, R. Zhang, R. Schober, D. W. K. Ng, D. I. Kim, and H. V. Poor, "Fundamentals of Wireless Information and Power Transfer: From RF Energy Harvester Models to Signal and System Designs," *IEEE J. Select. Areas Commun.*, vol. 37, no. 1, pp. 4–33, Jan. 2019.
- [12] X. Lu, P. Wang, D. Niyato, D. I. Kim, and Z. Han, "Wireless Networks with RF Energy Harvesting: A Contemporary Survey," *IEEE Commun. Surveys Tuts.*, vol. 17, no. 2, pp. 757–789, Second quarter 2015.
- [13] E. Boshkovska, D. Ng, N. Zlatanov, and R. Schober, "Practical Non-linear Energy Harvesting Model and Resource Allocation for SWIPT Systems," *IEEE Commun. Lett.*, vol. 19, no. 12, pp. 2082–2085, Dec. 2015.
- [14] J. Guo, H. Zhang, and X. Zhu, "Theoretical Analysis of RF-DC Conversion Efficiency for Class-F Rectifiers," *IEEE Trans. on Microwave Theory and Techniques*, vol. 62, no. 4, pp. 977–985, Apr. 2014.
- [15] S. Nikolettseas, Y. Yang, and A. Georgiadis, Eds., *Wireless Power Transfer Algorithms, Technologies and Applications in Ad Hoc Communication Networks*. Springer International Publishing, 2016.
- [16] A. Boaventura, A. Collado, N. B. Carvalho, and A. Georgiadis, "Optimum Behavior: Wireless Power Transmission System Design Through Behavioral Models and Efficient Synthesis Techniques," *IEEE Microwave Mag.*, vol. 14, no. 2, pp. 26–35, Mar. 2013.
- [17] M. R. V. Moghadam, Y. Zeng, and R. Zhang, "Waveform Optimization for Radio-Frequency Wireless Power Transfer," in *Proc. IEEE Intern. Workshop on Signal Process. Adv. in Wireless Commun. (SPAWC)*, Jul. 2017, pp. 1–6.
- [18] B. Clerckx and E. Bayguzina, "Waveform Design for Wireless Power Transfer," *IEEE Trans. Signal Process.*, vol. 64, no. 23, pp. 6313–6328, Dec. 2016.
- [19] R. G. Harrison and X. L. Polozec, "Nonsquarelaw Behavior of Diode Detectors Analyzed By The Ritz-Galerkin Method," *IEEE Trans. on Microwave Theory and Techniques*, vol. 42, no. 5, pp. 840–846, May 1994.
- [20] W. Shockley, "The Theory of P-N Junctions in Semiconductors and P-N Junction Transistors," *Bell System Tech. J.*, vol. 28, no. 3, pp. 435–489, Jul. 1949.
- [21] C. E. Shannon, "A Mathematical Theory of Communication," *Bell System Tech. J.*, vol. 27, no. 3, pp. 379–423, 1948.
- [22] J. G. Smith, "The Information Capacity of Amplitude- and Variance-Constrained Scalar Gaussian Channels," *Inf. and Control*, vol. 18, no. 3, pp. 203–219, 1971.
- [23] S. Shamai and I. Bar-David, "The Capacity of Average and Peak-Power-Limited Quadrature Gaussian Channels," *IEEE Trans. Inf. Theory*, vol. 41, no. 4, pp. 1060–1071, Jul. 1995.
- [24] M. Varasteh, B. Rassouli, and B. Clerckx, "On Capacity-Achieving Distributions for Complex AWGN Channels Under Nonlinear Power Constraints and their Applications to SWIPT," *ArXiv e-prints*, Dec. 2017, arXiv:1712.01226.
- [25] I. C. Abou-Faycal, M. D. Trott, and S. Shamai, "The Capacity of Discrete-Time Memoryless Rayleigh-Fading Channels," *IEEE Trans. Inf. Theory*, vol. 47, no. 4, pp. 1290–1301, May 2001.
- [26] J. J. Fahs and I. C. Abou-Faycal, "Using Hermite Bases in Studying Capacity-Achieving Distributions Over AWGN Channels," *IEEE Trans. Inf. Theory*, vol. 58, no. 8, pp. 5302–5322, Aug. 2012.
- [27] N. Zlatanov, E. Sippel, V. Jamali, and R. Schober, "Capacity of the Gaussian Two-Hop Full-Duplex Relay Channel With Residual Self-Interference," *IEEE Trans. Commun.*, vol. 65, no. 3, pp. 1005–1021, Mar. 2017.
- [28] Le Polozec, Xavier, "Input Impedance of Series Schottky Diode Detector at Low and High Power," May 2015, DOI:10.13140/RG.2.1.4530.9600.
- [29] R. M. Corless, G. H. Gonnet, D. E. G. Hare, D. J. Jeffrey, and D. E. Knuth, "On the LambertW Function," *Advances in Computational Mathematics*, vol. 5, no. 1, pp. 329–359, Dec. 1996.
- [30] K. Kim, H. Lee, and J. Lee, "Waveform Design for Fair Wireless Power Transfer With Multiple Energy Harvesting Devices," *IEEE J. Select. Areas Commun.*, vol. 37, no. 1, pp. 34–47, Jan. 2019.
- [31] T. Le, K. Mayaram, and T. Fiez, "Efficient Far-Field Radio Frequency Energy Harvesting for Passively Powered Sensor Networks," *IEEE J. of Solid-State Circuits*, vol. 43, no. 5, pp. 1287–1302, May 2008.
- [32] Skyworks Solutions, Inc., *SMS7630-061: Surface Mount, 0201 Zero Bias Silicon Schottky Detector Diode*, May 2015.
- [33] The Keysight Technologies, Inc., "Electronic Design Automation (EDA) Software, Advanced Design System (ADS), Version 2017."
- [34] M. Grant and S. Boyd, "CVX: Matlab Software for Disciplined Convex Programming, Version 2.0 Beta," Sep. 2012.
- [35] D. J. Jeffrey, G. A. Kalugin, and N. Murdoch, "Lagrange Inversion and Lambert W," in *Intern. Sympos. on Symbolic and Numeric Algorithms for Scientific Comput. (SYNASC)*, Sep. 2015, pp. 42–46.



Rania Morsi Rania Morsi (S'07) received the B.Sc. degree with highest honors from the faculty of Information Engineering and Technology (IET) at the German University in Cairo (GUC) in 2009. In 2010, she received the M.Sc. degree from the international Masters program "Communications Technology" at Ulm University, Germany. From February 2011 to July 2012, she was a teaching and research assistant at the GUC. Since August 2012, she is working toward the Ph.D. degree at the Institute of Digital Communications at the Friedrich-Alexander-University (FAU), Erlangen, Germany. Her research interests fall into the broad area of wireless communications including the field of energy harvesting and wireless power transfer.

Rania received a scholarship for her bachelor studies at the GUC. Her Master studies were sponsored by the German Academic Exchange Service (DAAD). In 2009, she ranked first in the B.Sc. degree over the faculty of IET in the GUC. In 2010, she received the second best student award at the Master program in Ulm University. Rania won the third best tutorial evaluation twice in FAU in 2012 and 2013 for teaching the "Digital Communications" master course.



Vahid Jamali (S'12) received the B.S. and M.S. degrees (honors) in electrical engineering from the K. N. Toosi University of Technology, Tehran, Iran, in 2010 and 2012, respectively, and the Ph.D. degree (with distinctions) from the Friedrich-Alexander-University (FAU) of Erlangen-Nürnberg, Erlangen, Germany, in 2019. In 2017, he was a Visiting Research Scholar with Stanford University, CA, USA. He is currently a Postdoctoral Fellow with the Institute for Digital

Communication, FAU. His research interests include wireless and molecular communications, Bayesian inference and learning, and multiuser information theory.

Dr. Jamali received several awards, including the Exemplary Reviewer Certificates IEEE COMMUNICATIONS LETTERS in 2014 and the IEEE TRANSACTIONS ON COMMUNICATIONS in 2017 and 2018, the Best Paper Award from the IEEE International Conference on Communications in 2016, the Doctoral Scholarship from the German Academic Exchange Service (DAAD) in 2017, and the Goldener Igel Publication Award from the Telecommunications Laboratory (LNT), FAU, in 2018. He has served as a member of the Technical Program Committee for several IEEE conferences and is currently an Associate Editor of IEEE COMMUNICATIONS LETTERS and IEEE OPEN JOURNAL OF COMMUNICATIONS SOCIETY.



Amelie Hagelauer Amelie Hagelauer (S'08-M'10-SM'18) received the Dipl.-Ing. degree in mechatronics and the Dr.-Ing. degree in electrical engineering from the Friedrich-Alexander-University Erlangen-Nuremberg, Germany in 2007 and 2013, respectively. She has been a professor at Universität Bayreuth since Aug 2019. Prior to that, she joined the Institute for Electronics Engineering in November 2007, where she was working on thin film BAW filters towards her Ph.D. Since

2013 she is focusing on SAW/BAW and RF MEMS components, as well as integrated circuits for frontends up to 180 GHz. Dr. Hagelauer has been the Chair of MTT-2 Microwave Acoustics from 2015 - 2017. She is continuously contributing to the development of RF Acoustics community by organizing workshops and student design competitions. She has been acting as Associate Editor of the IEEE MTT Transactions, as Guest Editor for a special issue of the IEEE MTT Transactions on the topic "RF Frontends for Mobile Radio" as well as for a special issue in the MDPI Journal Sensors on the topic "Surface Acoustic Wave and Bulk Acoustic Wave Sensors".



Derrick Wing Kwan Ng (S'06-M'12-SM'17) received the bachelor degree with first-class honors and the Master of Philosophy (M.Phil.) degree in electronic engineering from the Hong Kong University of Science and Technology (HKUST) in 2006 and 2008, respectively. He received his Ph.D. degree from the University of British Columbia (UBC) in 2012. He was a senior postdoctoral fellow at the Institute for Digital Communications, Friedrich-Alexander-University

Erlangen-Nürnberg (FAU), Germany. He is now working as a Senior Lecturer and an ARC DECRA Research Fellow at the University of New South Wales, Sydney, Australia. His research interests include convex and non-convex optimization, physical layer security, wireless information and power transfer, and green (energy-efficient) wireless communications.

Dr. Ng received the Best Paper Awards at the IEEE TCGCC Best Journal Paper Award 2018, INISCOM 2018, IEEE International Conference on Communications (ICC) 2018, IEEE International Conference on Computing, Networking and Communications (ICNC) 2016, IEEE Wireless Communications and Networking Conference (WCNC) 2012, the IEEE Global Telecommunication Conference (Globecom) 2011, and the IEEE Third International Conference on Communications and Networking in China 2008. He is now serving as an area editor for IEEE Open Journal of the Communications Society, an editor for IEEE Transactions on Wireless Communications, IEEE TGCN, IEEE Open Journal of Vehicular Technology, and a guest editor of IEEE JSAC Multiple Antenna Technologies for Beyond 5G, IEEE JSAC Massive Access for 5G and beyond. Besides, he has been serving as an editorial assistant to the Editor-in-Chief of the IEEE Transactions on Communications since Jan. 2012. In addition, he is listed as a Highly Cited Researcher by Clarivate Analytics in 2018 and 2019.



Robert Schober Robert Schober (S'98, M'01, SM'08, F'10) was born in Neuendettelsau, Germany, in 1971. He received the Diplom (Univ.) and the Ph.D. degrees in electrical engineering from Friedrich Alexander University (FAU), Erlangen, Germany in 1997 and 2000, respectively. From May 2001 to April 2002 he was a Postdoctoral Fellow at the University of Toronto, Canada, sponsored by the German Academic Exchange Service (DAAD). From May 2002 to December 2011

he was a Professor and Canada Research Chair at the University of British Columbia (UBC), Vancouver, Canada. Since January 2012 he is an Alexander von Humboldt Professor and the Chair for Digital Communication at FAU. His research interests fall into the broad areas of Communication Theory, Wireless Communications, and Statistical Signal Processing.

Dr. Schober received several awards for his work including the 2002 Heinz MaierLeibnitz Award of the German Science Foundation (DFG), the 2004 Innovations Award of the Vodafone Foundation for Research in Mobile Communications, the 2006 UBC Killam Research Prize, the 2007 Wilhelm Friedrich Bessel Research Award of the Alexander von Humboldt Foundation, the 2008 Charles McDowell Award for Excellence in Research from UBC, a 2011 Alexander von Humboldt Professorship, and a 2012 NSERC E.W.R. Steacie Fellowship. In addition, he received several best paper awards for his research. Dr. Schober is a Fellow of the Canadian Academy of Engineering and a Fellow of the Engineering Institute of Canada. From 2012 to 2015 he served as Editor-in-Chief of the IEEE Transactions on Communications. Currently, he serves as the Chair of the Steering Committee of the IEEE Transactions on Molecular, Biological and Multiscale Communication, on the Editorial Board of the Proceedings of the IEEE, and on the Board of Governors of the IEEE Communication Society (ComSoc). He is also an IEEE ComSoc Distinguished Lecturer.